

## **General Disclaimer**

### **One or more of the Following Statements may affect this Document**

- This document has been reproduced from the best copy furnished by the organizational source. It is being released in the interest of making available as much information as possible.
- This document may contain data, which exceeds the sheet parameters. It was furnished in this condition by the organizational source and is the best copy available.
- This document may contain tone-on-tone or color graphs, charts and/or pictures, which have been reproduced in black and white.
- This document is paginated as submitted by the original source.
- Portions of this document are not fully legible due to the historical nature of some of the material. However, it is the best reproduction available from the original submission.

A VERSATILE DETECTOR SYSTEM TO  
MEASURE THE CHARGE STATES,  
MASS COMPOSITIONS AND ENERGY SPECTRA OF  
INTERPLANETARY AND MAGNETOSPHERE IONS\*

George Gloeckler

Department of Physics and Astronomy  
University of Maryland  
College Park, Maryland

TR 77-043  
PP 77-148

\* Supported in part by the National Aeronautics and Space Administration under grants NGR 21-002-224 and NGR 21-002-316.

**A VERSATILE DETECTOR SYSTEM TO  
MEASURE THE CHARGE STATES,  
MASS COMPOSITIONS AND ENERGY SPECTRA OF  
INTERPLANETARY AND MAGNETOSPHERE IONS\***

**George Gloeckler**

**Department of Physics and Astronomy  
University of Maryland  
College Park, Maryland**

**Abstract**

We describe an instrument which can measure in detail the mass and charge state composition as well as the energy spectra and angular distributions of 0.5 to 350 keV/charge ions in interplanetary space and in magnetospheres of planets such as Jupiter and earth. Electrostatic deflection combined with a time-of-flight and energy measurement allows three-parameter analysis of output signals from which the mass, charge states and energy are uniquely determined. Post-acceleration by 30 kV extends the energy range of the detector system into the solar wind and magnetosphere plasma regime. Isotopes of H and He are easily resolved as are individual elements up to Ne and the dominant elements up to and including Fe. This instrument has an extremely large dynamic range in intensity ( $\sim 2 \cdot 10^{14}$ ) and is sensitive to rare elements even in the presence of high intensity radiation. Because of these features and modest weight, power and telemetry requirements this instrument is particularly well adapted for interplanetary, deep-space and out-of-the ecliptic missions as well as for flights on spacecraft orbiting Jupiter and earth. Although of fundamental importance, composition measurements of the thermal and suprathermal plasmas in space are fragmentary and quite incomplete.

## I. INTRODUCTION

Measurements of the charge states and the chemical and isotopic compositions of particles originating in the galaxy, the sun, and the magnetospheres of earth and Jupiter are of fundamental importance (a) in identifying their sources of origin, (b) in characterizing regions in space in which they are confined and through which they propagate, and (c) in providing essential information on mechanisms responsible for their acceleration. Our knowledge on particle composition is most advanced for galactic cosmic rays (Meyer, 1975) and energetic solar particles (Gloeckler, 1975). Significant progress in these studies is just now beginning for low energy particles confined to or originating in the earth's magnetosphere (Fritz, 1976). Information on the abundances of thermal and suprathermal ions at Jupiter has not yet been obtained, and our knowledge of the chemical and charge state composition of solar wind ions is fragmentary and quite incomplete (Hirshberg, 1974, Eberhardt, 1974). These significant gaps in our knowledge of the composition of thermal ( $\sim 1$  keV/nuc) and suprathermal ( $\lesssim 300$  keV/nuc) ions of solar, interplanetary and magnetospheric origin exist because suitable detector systems were not available and have not been flown.

In this paper we describe a versatile instrument which can measure in detail the energy spectra, composition and charge states of low energy ions in interplanetary space and magnetospheres of planets, such as earth and Jupiter. This charge-energy-mass-spectrometer (CHEM) can be adapted to operate without degradation and to provide composition measurements of thermal and suprathermal ions in intense radiation environments, such as those encountered at Jupiter at  $6 R_J$ , or to measure the charge state and chemical composition of the solar wind. In particular, CHEM has the capability to detect and identify heavy ions whose intensities are as low as  $5 \cdot 10^{-4}$  or as high as  $10^{11}$   $(\text{cm}^2 \text{sec sr keV/nuc})^{-1}$  in the energy range between 0.5 and 350 keV/charge.

With the CHEM spectrometer it is possible to:

- (a) detect and identify protons, deuterons,  $\text{He}^3$ ,  $\text{He}^4$  and heavier ions in the energy range 0.5 to 350 keV/charge.
- (b) measure the energy spectra of individual ion species over the entire energy range with a resolution  $\Delta E/E$  of between 2 and 18%.
- (c) measure the charge states of these ions.
- (d) resolve unambiguously the isotopes of light elements (at least up to carbon) and analyze with high priority dominant elements up to and including iron, such as, for example, sodium, sulphur and potassium ions.

- (e) measure fluxes as low as  $5 \cdot 10^{-4}$  or as high as  $10^{11}$  ( $\text{cm}^2 \text{sec sr keV/nuc.})^{-1}$ .
- (f) perform composition measurements in intense radiation environments (for example, at Jupiter at  $6R_J$ ).
- (g) obtain composition measurements of heavy ions in the solar wind in the presence of large fluxes of solar wind protons.
- (h) analyze the composition and motions of ions in the outer cometary atmospheres.

The major advantages of the CHEM Spectrometer over other detector systems generally used include

- measurements in an energy range not accessible with standard techniques ( $dE/dx$  vs  $E$  detectors have a low energy limit of  $\sim 100$  keV/nuc no matter how thin the  $dE$  detector, while conventional plasma instruments generally stop at  $\sim 10$  to  $20$  keV/q).
- capability to measure simultaneously the charge state, mass and energy of the incoming ions. (Charge states are not measured by  $dE/dx$  vs  $E$ , time-of-flight techniques, or a combination of these two methods; conventional electrostatic and magnetic deflection detectors which rely on a simple threshold detector such as a channeltron can at best measure mass per charge and are sensitive to background radiation).
- extreme insensitivity to background and an extensive intensity dynamic range ( $\sim 2 \cdot 10^{14}$ ) achieved by a combination of electrostatic deflection "filtering" (not feasible at energies above  $\sim 0.5$  MeV/charge) and fast double and triple coincidence counting techniques (not used in conventional thermal and suprathreshold plasma instruments).
- capability to continue measurements of the charge states and composition of the thermal plasma during times of spacecraft charging to  $\sim 20$  KV.

## II. PRINCIPLE OF OPERATION

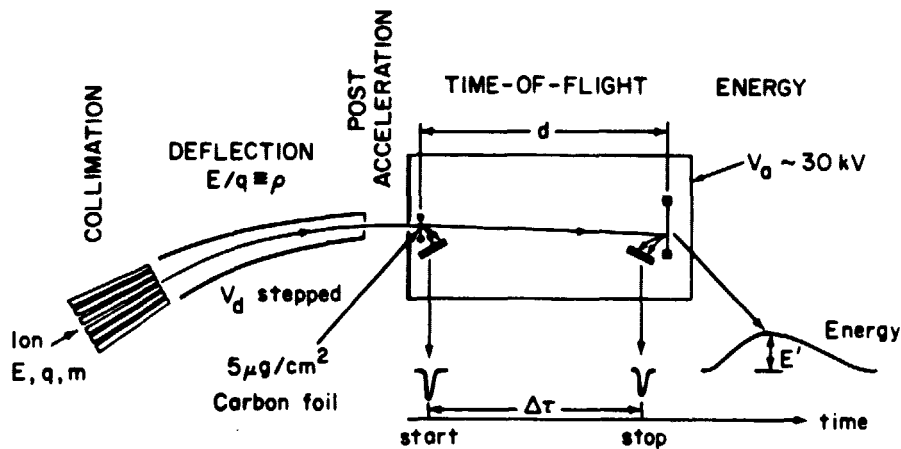
The CHEM Spectrometer is based on the proven technique of electrostatic deflection in combination with a time-of-flight and energy measurement. Fig. 1 shows a schematic representation of the instrument. A large area, multi-slit, focusing collimator defines the entrance trajectories of incoming ions, each characterized by its energy  $E$ , ionization (or charge) state  $q$ , and mass  $m$ .

The electrostatic deflection analyzer selects ions which have the same  $E/q$  ratios and allows these ions to enter the time-of-flight (TOF) system. The ratio of the slit width of the exit slit in the deflection system to the total amount of deflection determines the energy per charge

passband ( $\Delta E/q$ ), and the energy resolution  $\Delta E/E$  (typically 5 to 15%) of the analyzer. The  $E/q$  value is varied systematically by stepping the deflection voltage.

The time-of-flight system serves to measure the velocity of the ions. Two secondary electron detector assemblies (SEDA's) separated by a distance  $d$  ( $\sim 10$  cm) are used as the "start" and "stop" detector. From the time delay  $\Delta\tau$ , (typically 20-200ns) between the start and stop signals the velocity  $v$  may be determined which, along with the known value of  $E/q = \rho$  gives the mass to charge ratio  $m/q$  of the ion. The start SEDA consists of a thin ( $\sim 5\mu\text{g}/\text{cm}^2$ ) carbon foil and a microchannel plate (MCP) assembly. Ions passing through the carbon foil generate an abundant number ( $>10$ ) of secondary electrons in the surface layers of the carbon foil. These electrons are electrostatically focused onto the MCP which produces a fast timing signal. The carbon foil is thin enough so that the energy of the ion passing through it is not significantly degraded. The stop SEDA is identical to the start SEDA except that the surface gold layer of the solid state detector (which measures the energy of the ion) is used instead of the carbon foil to generate the secondary electrons.

### CHARGE-ENERGY-MASS (CHEM) SPECTROMETER



$$q = \frac{\alpha E'}{\rho} \quad m = 2\rho q \frac{\Delta\tau^2}{d^2} = 2\alpha E' \frac{\Delta\tau^2}{d^2} \quad E = \rho q = \alpha E'$$

Fig. 1 Schematic representation of the CHEM Spectrometer. The energy  $E'$  is measured with a solid state detector. Secondary electrons from the foil (start) and detector surface (stop) are detected using chevron microchannel plates.

The solid state detector (which is also part of the stop SEDA) measures the kinetic energy of the ion. This, combined with the measurement of velocity by the TOF system and the  $E/q \equiv \rho$  value of the deflection analyzer determines uniquely the charge state  $q$ , mass  $m$ , and energy  $E$  of the ions as indicated at the bottom of Fig. 1:  $q = \alpha E'/\rho$ ;  $m = 2\rho q(\Delta\tau)^2/d^2 = 2\alpha E'(\Delta\tau)^2/d^2$ ; and  $E = \rho q = \alpha E'$ . Energy losses in the carbon foil and the gold contact of the detector as well as non-ionizing collisions in the solid state detector (nuclear defect) combine to decrease the measured energy  $E'$  to a known fraction  $1/\alpha$  of energy  $E$  of the ion.

The lowest energy at which ions will penetrate the  $5\mu\text{g}/\text{cm}^2$  carbon foil of the start SEDA of TOF system is between 5 and 20 keV, and the lowest electronic threshold level on the signal of the solid state detector is 15 keV. Analysis of the ion composition below these energies (for example at several hundred eV), is achieved by post-accelerating the ions after they pass the electrostatic analyzer but prior to their entrance into the TOF system. A 30 kV post-acceleration is required in order to extend the energy range into the thermal plasma region (few hundred eV/nuc).

The powerful multi-parameter analysis technique, fully developed in cosmic ray and solar particle  $dE/dx$  vs  $E$  telescopes, is also applicable in the present case. In Fig. 2 we show a "matrix" of the time-of-flight vs energy for a given value of  $\rho = 20 \text{ keV}/q$ . We have, for the moment, neglected energy

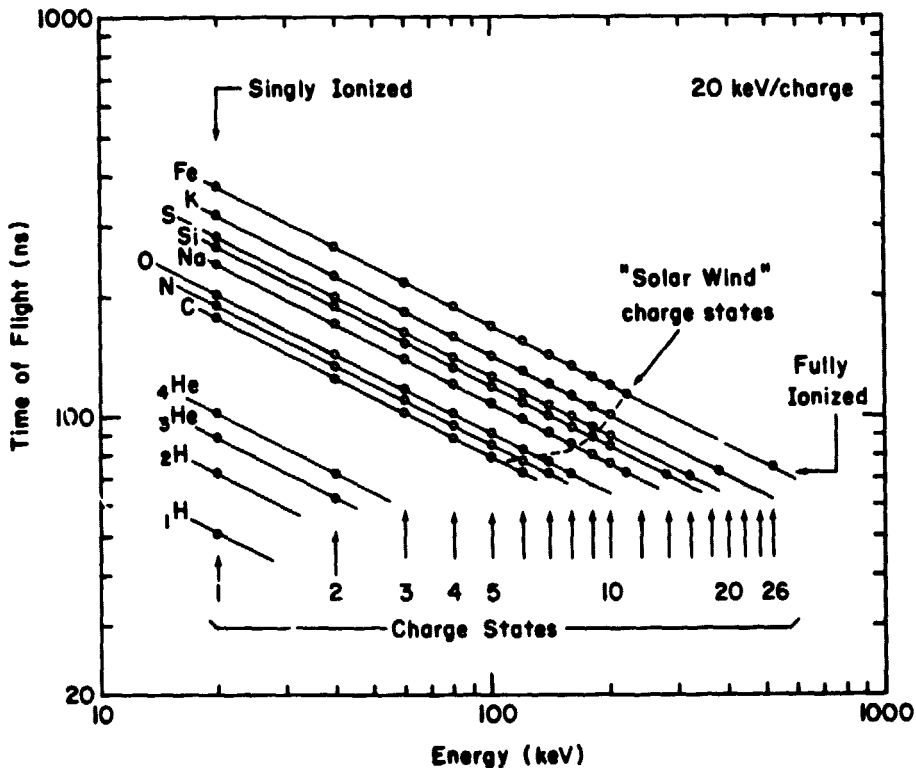


Fig. 2 Simplified Time-of-Flight vs Energy matrix.  $\circ$  and  $\circ$  indicate the locations of ions in this matrix.

losses of the ions and the nuclear defect in the solid state detector in order to simplify the discussion of the main features of the matrix. In this matrix display each charge state of each element has a unique position which is determined by the intersection of the respective "charge state" lines (vertical,  $E = q\rho$ ) and "mass" or "chemical element" lines (slope  $-1/2$ ). For example, all singly ionized particles lie at the intersection of the  $E = 20$  keV vertical line and the respective "mass" lines. The positions of a representative sample of charge states and elements are indicated as open and solid circles. The solid circles represent singly ionized particles, fully stripped nuclei and ions with charge state characteristic of the quiet solar wind. One should note in particular the wide separation between charge states and isotopes of H and He.

The advantages of two-parameter data analysis techniques are many, including

- (a) identification and isolation of any residual background; such residual background may be reliably corrected for.
- (b) identification and correction of any long term drifts; the positions of all elements would shift systematically.
- (c) self calibration of the detector system; the basic pattern of positions of the dominant elements and charge states is easy to recognize without precise knowledge of the locations of the individual elements.
- (d) applicability of statistical techniques to provide a determination of the relative abundances of neighboring elements and/or charge states which on an event by event basis could not be resolved from one another.

A matrix similar to that shown in Fig. 2 is obtained for each voltage step ( $\rho$  value) of the deflection analyzer. As  $\rho$  increases, the positions of each charge state of each element slides down and towards the right along the "mass" lines to new locations (the intersections of the new  $E = \rho q$  lines with "mass" lines"). A dynamic range in energy of 10 may be analyzed in contiguous intervals by increasing the voltage in 50 (or 16) steps by an amount  $\Delta E/E = 0.05$  (or 0.15), where  $\Delta E/q$  is the energy passband of the deflection analyzer.

### III. MEASURED RESPONSE OF THE TIME-OF-FLIGHT SYSTEM

The deflection analyzer with the large area multi-slit focusing collimator and high voltage deflection supplies is a fully developed system which was first flown as an integral part of the University of Maryland Experiments on the IMP 7 and 8 spacecraft (Tums et al., 1974). For the CHEM spectrometer one can adapt with only minor modifications the design of the stepped voltage deflection analyzer used in the Max-Planck/Maryland experiments on the International Sun-Earth Explorer satellites.

The time-of-flight technique using secondary electron detection to establish the start and stop times for ions traversing the system has been used for mass identification in low energy nuclear physics by many groups (Schneider, *et al.*, 1970, Goulding and Harvey, 1975 and references therein). We have modified the Berkeley design (Viola, 1975) of the secondary electron detector assembly (SEDA) for space-flight application and during the past two years have studied its characteristics. The results of these studies and calibrations of a prototype time-of-flight vs energy detector are summarized below.

#### Total Energy Measurements of Low Energy Heavy Ions (Nuclear Defect)

Energy losses of heavy ions in the gold contact layer of a solid state detector and non-ionizing nuclear collision of the ions in the silicon lattice reduce the fraction of the incident energy measured by these devices. At high energies ( $\gtrsim 1$  MeV/nuc) these effects are small and over 95% of the incident energy is detected. At lower energy the fraction of the incident energy measured decreases reaching values of about 0.2 for Kr at 1 keV/nucleon. Not only are there few measurements of the response of solid state detectors to low energy heavy ions, but there is also a large degree of inconsistency among the published values. Since some of the differences may be attributed to differences among the solid state detectors used (some detectors are known to have additional "dead" layers of Si) we have undertaken a series of measurements of energy losses of heavy ions in solid state detectors fabricated in our laboratory. The results are shown in Fig. 3 for  $^1\text{H}$ ,  $^2\text{H}$ ,  $^4\text{He}$ ,  $^{12}\text{C}$ ,  $^{14}\text{N}$ ,  $^{16}\text{O}$ ,  $^{20}\text{Ne}$ ,  $^{40}\text{Ar}$  and  $^{84}\text{Kr}$  in the energy range from  $\sim 2$  to 400 keV/nucleon. The upper curve in each panel represents calculated responses based on the Lindhard, *et al.* (1963) theory of nuclear defect; the lower curve is based on calculations which combine nuclear defect with energy losses (Northcliffe and Schilling, 1970) of the ions in the  $19\mu\text{g}/\text{cm}^2$  gold layer of our detectors. For elements up through oxygen the agreement with theoretical predictions is excellent; for heavier ions deviations from the calculated curves are evident. (A full discussion of these results is given by Ipavich *et al.*, [1977]). Using these measurements we have constructed measured energy vs incident energy response curves for particles with energies between 1 and 1000 keV/nucleon covering a mass range between 1 and 84 amu. A sample is shown in Fig. 4, where the heavy curves represent best fits to our measurements and the light curves are extrapolations of our data using theoretical models of nuclear defects and electronic stopping power (Lindhard, *et al.*, 1963; Northcliffe and Schilling, 1970) in gold and silicon.

Fig. 5 shows the measured FWHM energy spread vs incident kinetic energy of the ions in solid state detectors. The curves represent best fits to the data points. Amplifier noise of 12 keV FWHM has not been subtracted from these data.

#### Energy Losses of Heavy Ions in Carbon

Measurements of stopping powers and ranges in carbon for a variety of heavy ions have been published (Ormrod and Duckworth, 1963; Högberg, 1971;

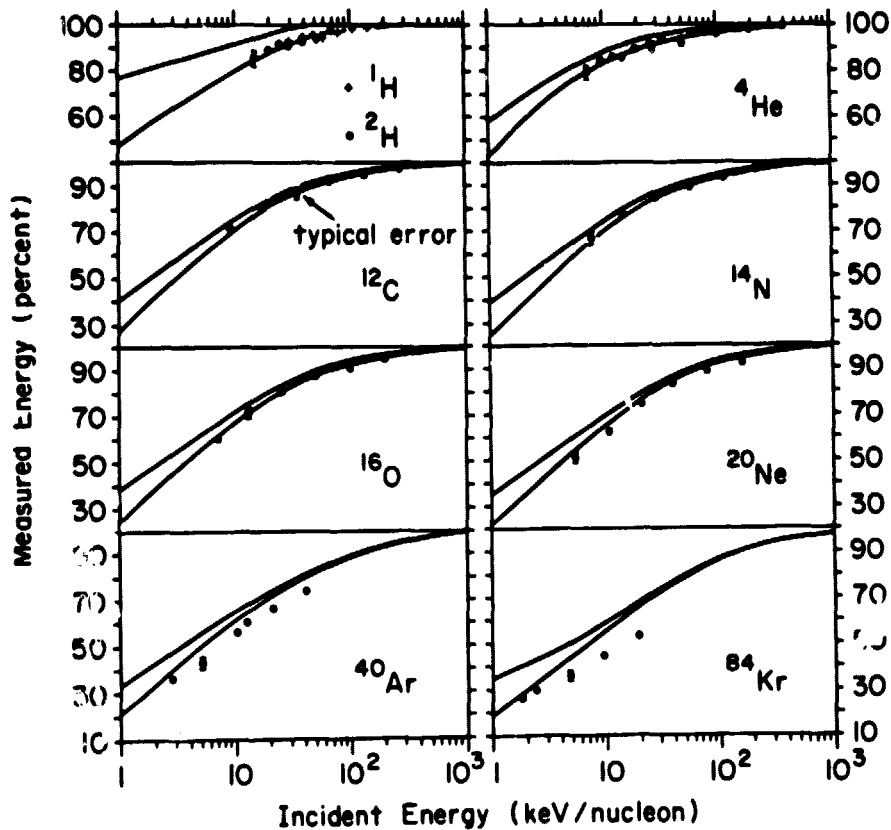


Fig. 3 Measured energy defect of H through Kr in the University of Maryland solid state detectors.

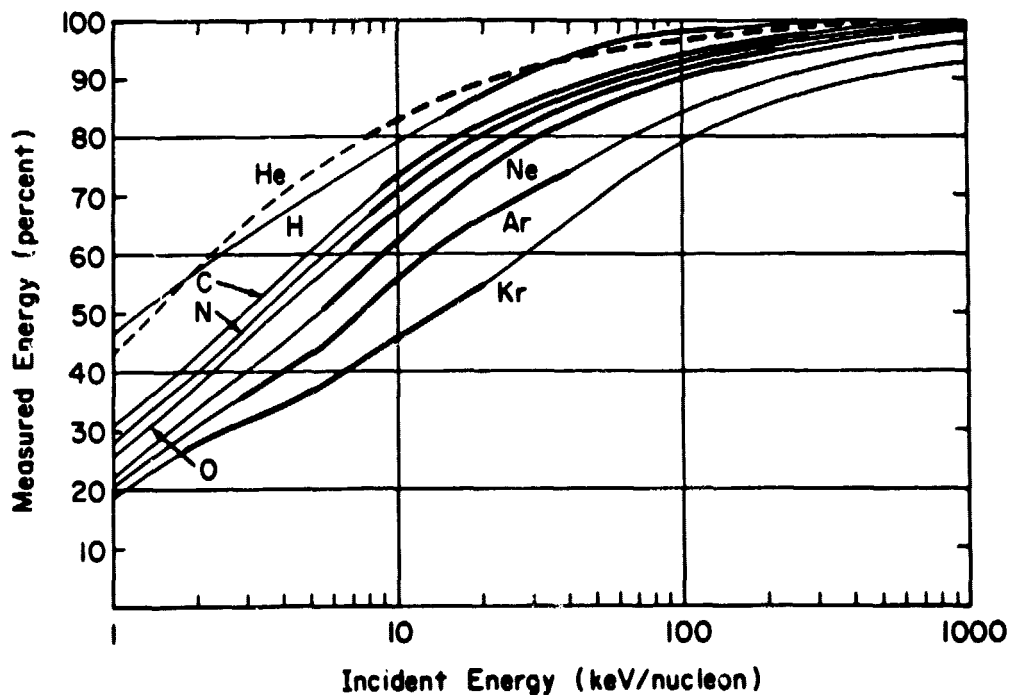


Fig. 4 Total energy defect in solid state detectors for H through Kr between 1 and 1000 keV/nucleon. Heavy curves represent least squares fits to the data of Fig. 3.

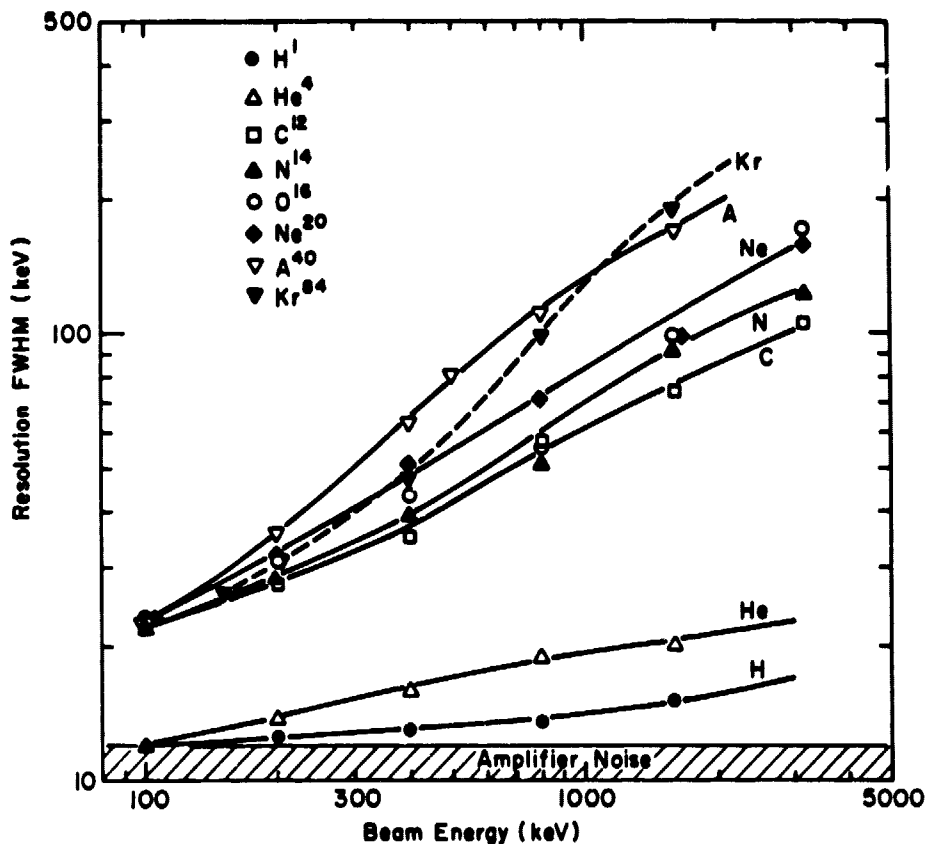


Fig. 5 Measured energy resolution (FWHM) as a function of incident particle energy in the University of Maryland solid state detectors.

Powers and Whaling, 1962; Chu, *et al.*, 1968; Bernstein, *et al.*, 1970; Wijngaarden and Duckworth, 1962). In Fig. 6 we show for various ions energy loss curves which fit these data at low energies ( $\lesssim 10$  keV/nuc) and merge with calculated curves of the total stopping powers derived from the range-energy tables of Northcliffe and Schilling (1970) at higher energies.

For N and H we also show indirect measurements of Hsieh (1976) based on time-of-flight analysis of field-ionized and accelerated molecules. Although the nitrogen data is in good agreement with the curves shown, the stopping powers for H seem to lie a factor of 2 above the values indicated by the curve. The important points to note, however, are that the energy losses (a) are at most several keV/ $\mu\text{g}/\text{cm}^2$  at  $\sim 1$  keV/nucleon, (b) decrease with decreasing energy and (c) depend only weakly on the ion energy.

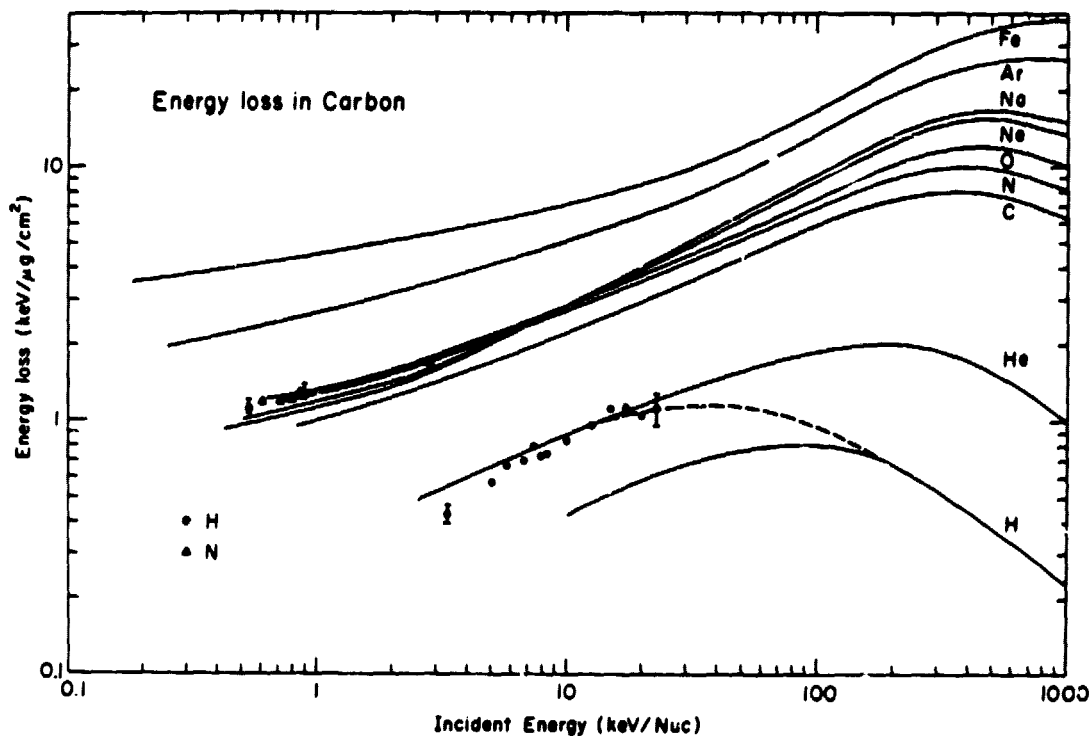


Fig. 6 Energy loss curves for various ions in carbon foils.

#### Response of the Secondary Electron Detector Assemblies to Charged Particles

We have investigated the pulse shapes, pulse height distributions and detection efficiencies of the secondary electron detector assemblies (SEDA's) using Van de Graaff beams of electrons, protons and heavy ions. The SEDA's we used consist of a  $5 \mu\text{g}/\text{cm}^2$  carbon foil (or solid state detector surface), accelerating and deflection electrode grids, and microchannel plates (Green et al., 1975) mounted in a chevron arrangement (Washington, 1973). Secondary electrons having energies of  $\sim 10$ -100 eV are generated by an ion penetrating the carbon foil (or by an ion impinging on the surface of the solid state detector). These electrons are then accelerated to 1 keV and focused by curved deflection grids onto the surface of the first microchannel plate (see Fig. 12 for a cross sectional view of the SEDA's). The chevron assembly for the MCP is used to eliminate ion feedback (Washington, 1973) and is biased to run at a gain between  $10^6$  and  $10^7$ .

The shape and most probable amplitude of the output pulse from the MCP assembly triggered by passage of 400 keV nitrogen ions passing through the SEDA is shown in Fig. 7. The pulse amplitude is about 0.5 volts and the duration of the pulse  $\sim 2$  ns. We shall show below that pulse of such large amplitude and fast rise time greatly reduce the complexity, weight and power

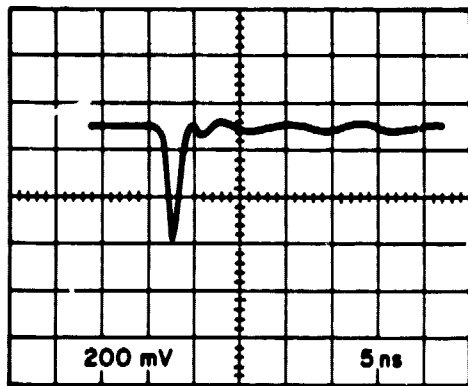
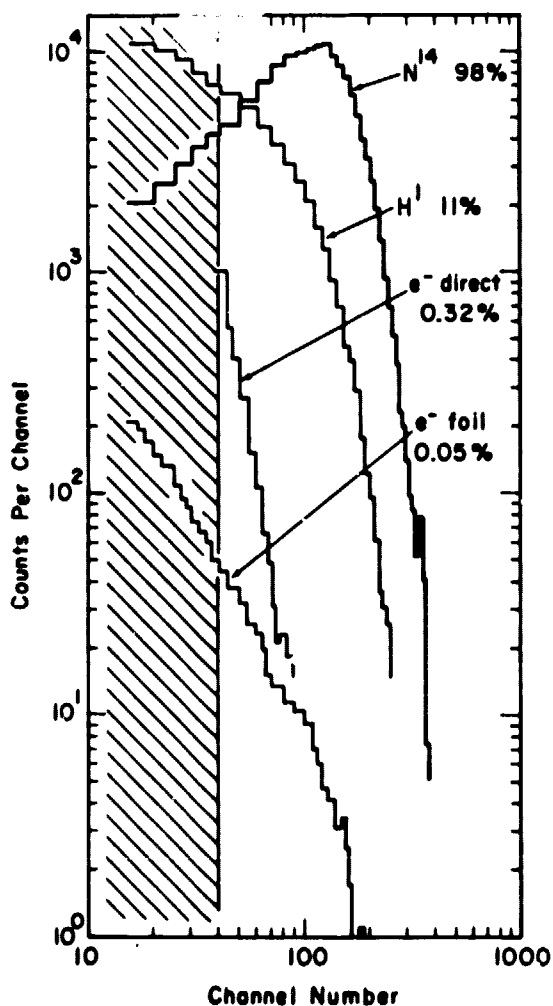


Fig. 7 Shape and amplitude of the output signal of the secondary electron detector assembly (SEDA) exposed to a 400 keV  $N^+$  beam.

requirements of the TOF electronics. Using the measured pulse amplitude and duration we can estimate the number of secondary electrons focused onto the MCP assembly. The total charge collected is  $q = i\Delta\tau = (V/R)\Delta\tau = 2 \cdot 10^{-11}$  Coulomb. The average number of electrons detected at a gain of  $5 \cdot 10^6$  is 25 which is in reasonable agreement with expected values (Clerc et al., 1973).



To study the efficiency of detecting various particles either directly in the MCP's or through secondary electrons, we pulse-height-analyzed the MCP outputs during passage of beams of electrons, protons and heavy ions through the SEDA assembly. The pulse-height spectra for 400 keV electrons, protons and nitrogen are shown in Fig. 8. These spectra have been normalized relative to one another using the counting rate of the beam monitor detector.

Fig. 8 Pulse-height spectra of the output signal from a SEDA exposed to 400 keV  $H$ ,  $N^+$  and electrons. The spectrum labeled " $e^-$  direct" refers to the direct exposure of the microchannel plate to electrons.

The large differences in the shapes of the spectra are clearly evident. While the nitrogen spectrum shows a distinct peak at channel  $\sim 120$ , the spectra for electrons have power law forms with exponents  $-6$  and  $-2$  respectively. More important is the fact that the detection efficiency above a given threshold for heavy ions far exceeds that for electrons and protons. This is directly related to the lower secondary electron yield of low-mass particles. If we set a threshold at channel 40 (corresponding to about 150 mV) then 98% of nitrogen (and a similarly large fraction of other heavy ions) would be detected compared with 11% of protons and only 0.05% of electrons passing through the foil. The fraction of electrons hitting the MCP directly and producing pulse amplitudes exceeding 150 mV is 0.3%. We note here that MCP gain shifts by a factor of 2 would not significantly affect the detection efficiency for heavy ions.

### Calibration of the Time-of-Flight vs Energy Detector System

Knowing the energy losses in carbon foils and the energy defect in solid state detectors it is possible to calculate the expected positions of each charge state of each element in the  $\Delta\tau$  vs E matrix. In Fig. 9 we show the predicted locations in the  $\Delta\tau$  vs E plane (for  $\rho = 25$  keV/q) for a representative sample of charge states and elements. For each point the FWHM limits in the measured energy and time are indicated as error bars and the charge state is given by the number next to the point. This display is, of course, similar to that of Fig. 2. The "elements" or "mass" lines still are of the form  $\Delta\tau \propto E^{-n}$  where  $n$  is now  $\sim 0.4$ . Despite the large uncertainties in the measurement of energy (these uncertainties are decreased at higher  $\rho$  values) one can readily separate all isotopes and charge states of H and He and resolve the dominant elements (such as C, O, Si, Fe) and charge states (fully stripped vs "solar wind" charge states, for example). With accumulation of data and statistical analysis of the distribution in the matrix, further improvements in the resolution will be achieved.

Two additional points deserve to be mentioned. First, even in the absence of a signal from the energy detector, the TOF measurement will unambiguously resolve singly-ionized elements (such as  $C^+$ ,  $N^+$ ,  $O^+$ ,  $Na^+$ ,  $S^+$ ,  $K^+$ ). Second, by discriminating on a signal  $S = \Delta\tau + a \cdot E$ , where  $\Delta\tau$  and  $E$  are the TOF and energy signals and "a" is a constant, it is possible to analyze only elements heavier than protons or heavier than He. For example, the threshold level shown by the dashed line in Fig. 9, clearly separates H and He from C and heavier ions.

We have calibrated a prototype time-of-flight vs energy detector system using Van de Graaff beams of  $^1H$ ,  $^3He$ ,  $^4He$ ,  $^{12}C$ ,  $^{14}N$ ,  $^{16}O$ ,  $^{20}Ne$  and  $^{40}Ar$ . The detector system consisted of the two SEDA's described above separated by 10 cm for the time-of-flight determination, and a University of Maryland solid state detector for the energy measurement. Commercial fast-time electronics were used for the TOF measurement. The  $\Delta\tau$  and the E signals were separately pulse-height analyzed. From the pulse-height spectra we determined the mean values and FWHM values for the  $\Delta\tau$  and E signals for each ion at each energy. The combined results of two calibration runs (open and solid symbols) are given in Fig. 10. The curves represent the calculated response taking into account energy losses in the carbon foil and gold layer and the nuclear defect in the solid state detector.

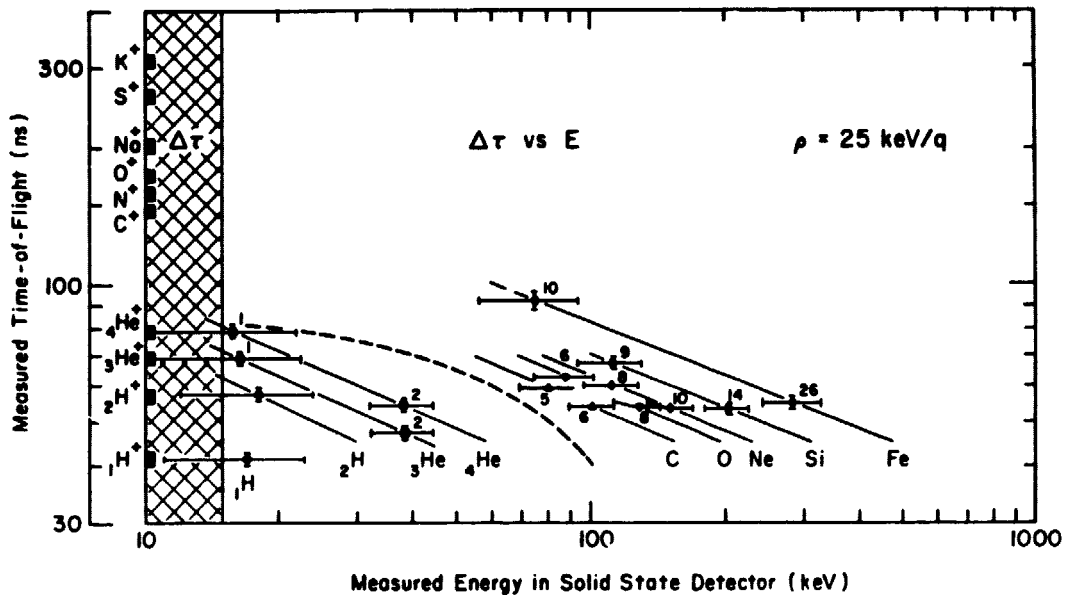


Fig. 9 Calculated positions of representative charge states and elements in the  $\Delta\tau$  vs E plane. The shaded region indicates one-dimensional time-of-flight ( $\Delta\tau$ ) analysis in the absence of an energy signal.

#### IV. DESCRIPTION OF THE CHEM SPECTROMETER

On the basis of our calibration experience with the time-of-flight system, thin carbon foils and microchannel plates, and our flight experience with deflection analyzers, high voltage supplies and solid state detectors, we have designed the Charge-Energy-Mass (CHEM) Spectrometer not only to work effectively and reliably in space but also to operate properly in high intensity radiation environments.

The energy and mass range covered by the CHEM Spectrometer is given in Fig. 11 in which three regions in the mass vs incident energy plane are drawn. Regions A and B indicate the response of the CHEM Spectrometer without post-acceleration. In region A, which extends from  $\sim$  few to  $\sim$ 200 keV/nucleon and includes element H to Fe, three-parameter analysis leads to the unambiguous identification of mass, charge state and energy of incoming ions. In region B, three-parameter analysis is made for all elements with charge states equal to or greater than indicated by the number next to the given element. (For example for potassium, three-parameter analysis is made for charge states of 5 and above.) For lower charge states the TOF measurement is made in the absence of the energy measurements, which still permits a determination of the ion composition based on unambiguous measurements of the  $m/q$  ratio of the ions. In particular, the composition of singly ionized particles such as  $\text{Na}^+$ ,  $\text{K}^+$ , and  $\text{S}^+$  is readily established. With post-acceleration of  $\sim$ 30 kV, three

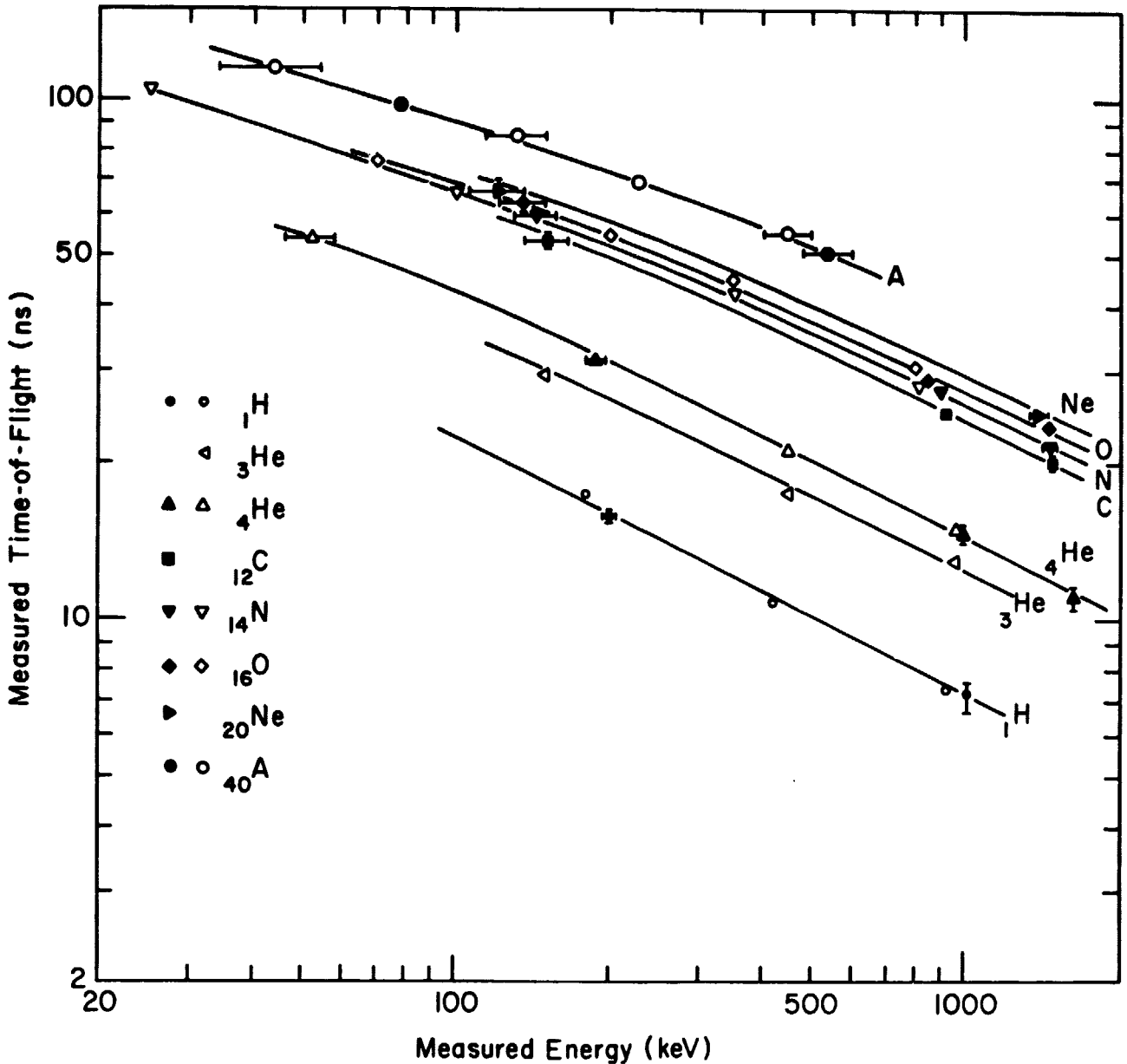


Fig. 10 Measured response of a prototype Time-of-Flight vs Energy Detector exposed to various ion beams. The flight path was 10 cm. Note the clear separation of the isotopes  $^3\text{He}$  and  $^4\text{He}$ .

parameter analysis (as in region A) is made for all charge states of all ions which lie in regions A, B or C. In particular, the chemical, isotopic and charge state composition of the solar wind and magnetosphere thermal plasma is measured.

# CHARGE-ENERGY-MASS (CHEM) SPECTROMETER

15052

## 3 PARAMETER ANALYSIS

### CHARGE STATE, MASS and ENERGY

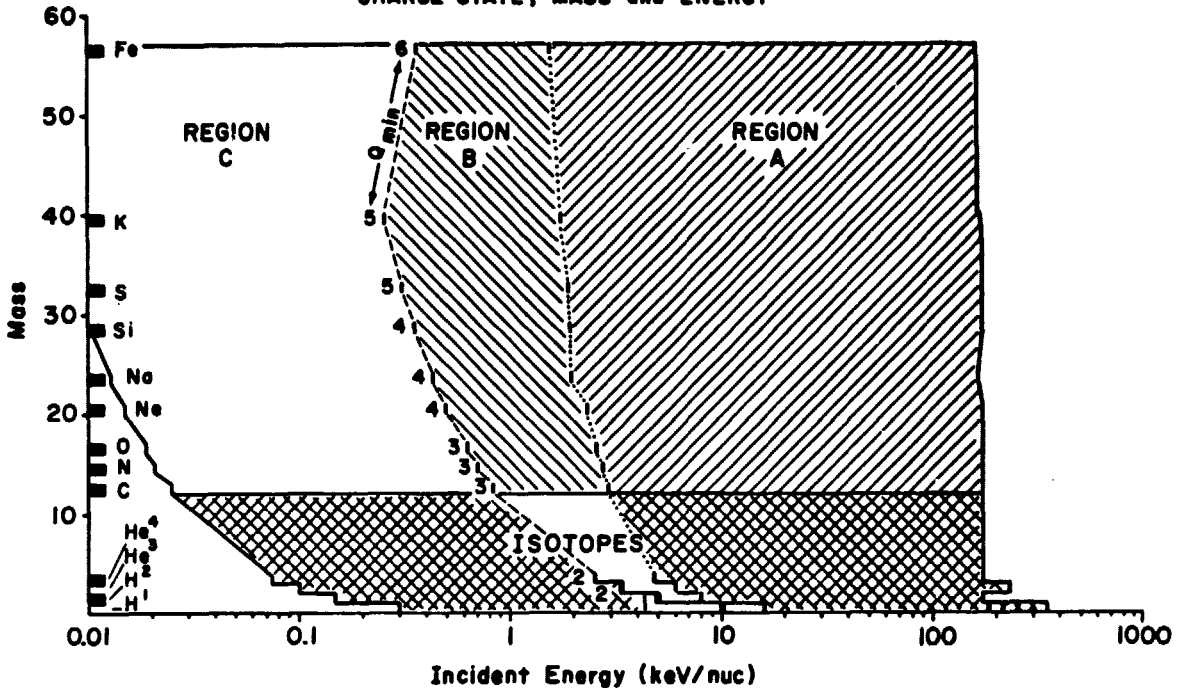


Fig. 11 Energy and mass range of the CHEM Spectrometer. Extension into region C is obtained by adding post-acceleration of  $\sim 30$  kV.

At any given time, the CHEM spectrometer will record a two-point differential energy spectrum of the individual isotopes and charge states of H and He as well as of the major charge states of elements beyond He. With the sensor located such that it looks perpendicular to the spacecraft spin axis and has an unobstructed field of view of  $40^\circ$  by  $50^\circ$ , two-dimensional pitch angles distributions of suprathermal particles in 16 angular sectors can be measured. Because of priority selection, immunity of the CHEM Spectrometer to background radiation and high sensitivity to thermal and suprathermal ions (which increases as the energy of incoming ions increases) it is possible to analyze the energy spectra and composition of rare isotopes, elements and charge states (deuterium for example). At the same time fast counting techniques (inherent in the TOF measurement) allow analysis of very intense fluxes of ions. These features combine to make the intensity dynamic range of the CHEM spectrometer  $\sim 2 \cdot 10^{14}$ . The charge and mass resolution, geometrical factors and sensitivity, intensity dynamic range, view angles and view direction of the CHEM sensor on a spinning spacecraft are summarized in Table 1.

### Mechanical Design

The cross sectional view of the CHEM sensor without post-acceleration and showing only the essential components is given in Fig. 12. The overall dimensions of the sensor and its fast analog electronics are  $24 \times 11 \times 16$  cm, and its weight is approximately 2000 gm.

TABLE 1  
Capabilities and Requirements of the CHEM Spectrometer

A. CAPABILITIES

- Energy resolution, $\Delta E/E$ :	$0.05 E \lesssim 70 \text{ keV}/q$ $0.02 \text{ to } 0.18 \text{ for } E \gtrsim 70 \text{ keV}/q$
- Charge and mass resolution:	Resolves all <u>charge states</u> and <u>isotopes</u> of H and He; resolves major elements and charge states up to and including Fe.
- Sensitivity (minimum detectable flux level):	$\sim 10^{-1}/\rho \text{ ions}/(\text{cm}^2 \text{ sec sr keV}/\text{charge})$ [ $\rho \equiv \text{energy}/\text{charge}$ in keV]
- Maximum Intensity:	$10^{11} \text{ ions}/(\text{cm}^2 \text{ sec sr keV}/\text{charge})$
- Geometrical factor, G:	$2 \cdot 10^{-3}$ and $10^{-3} \text{ cm}^2 \text{ sr}$
- Intensity dynamic range:	$2 \cdot 10^{14}$

B. REQUIREMENTS\*

- Weight	$\sim 2000 \text{ gm}$
- Power	$\sim 2500 \text{ mW}$
- Size	$24 \times 11 \times 16 \text{ cm}$
- View direction	Perpendicular to spin axis
- View angles	$40^\circ$ (in plane containing spin axis of spacecraft) $50^\circ$ (in equatorial plane of spacecraft)

\* DPU not included.

The deflection analyzer is made up of two deflection regions (high and low energy), each with its own multi-slit focusing collimator. The center deflection plate assembly, common to both deflection regions, is connected to the deflection voltage supply which increments the voltage from 430 to 3,000 V in up to 64 logarithmically spaced steps. A 1 mm exit slit in each deflection region defines the total deflection and the exit direction of the ions, as well as the energy resolution of the analyzer (5% and 18% for the low and high energy regions respectively). The deflection voltage supply is a simplified version of one which will fly in the MPI/University of Maryland ISEE A and C experiments. The multi-slit focusing collimators are direct adaptations of the University of Maryland experiments on the IMP 7 and 8 Spacecraft (Tums et. al, 1974)

The TOF vs E detector follows directly the deflection analyzer as shown in Fig. 12. The entire assembly may be shielded from all directions against  $\lesssim 10 \text{ MeV}$  electrons and  $\lesssim 55 \text{ MeV}$  protons to insure operation in high radiation intensity environments, such as at Jupiter at  $6R_J$ . The TOF system consists

## CHARGE-ENERGY-MASS (CHEM) SPECTROMETER

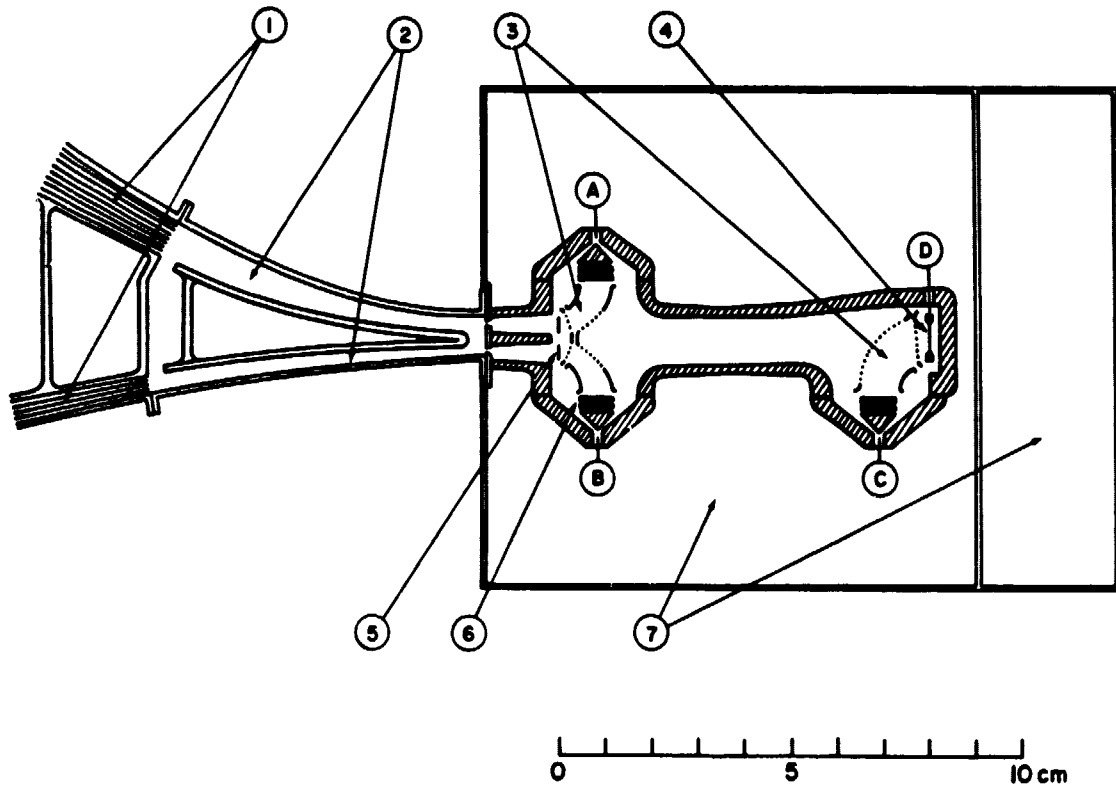


Fig. 12 Simplified cross sectional view of the CHEM sensor. (1) Multi-slit focusing collimator; (2) electrostatic deflection analyzer; (3) acceleration and deflection grids; (4) rectangular solid state detector; (5) carbon foils; (6) chevron microchannel plate assemblies; (7) housings for fast electronics. The shaded area represent 5.5 gm/cm<sup>2</sup> shielding of the TOF vs E sensor from all directions.

of two identical "start" secondary electron detector assemblies (SEDA's A and B) and a common "stop" SEDA (C), incorporating the surface of a rectangular solid state detector (D) for generating the secondary electrons. (We have verified in our laboratory the performance of the "stop" SEDA). The separation between the carbon foils and the solid state detector surface (the flight-path) is 8 cm. Each start SEDA consists of a 0.2 x 1 cm grid supported thin carbon foil, and acceleration and deflection grids for focusing the secondary electrons onto the front surface of a rectangular chevron microchannel plate assembly. The thickness of the carbon foil looking at the exit slit of the low energy deflection region is about 5 $\mu$ g/cm<sup>2</sup>, while the thickness of the other foil is 10 to 15 $\mu$ g/cm<sup>2</sup>. (2 $\mu$ g/cm<sup>2</sup> carbon foils have been flown on rocket experiments, [Bernstein *et al.* 1969a, b]). The stop SEDA consists of a 0.7 x 1.2 cm, 300 $\mu$ m thick rectangular surface barrier detector, the acceleration and deflection grids and a rectangular chevron microchannel plate assembly. The carbon foils and solid state detector are floated at -3.5 KV, the acceleration grids and the front surface of the multichannel plates are at -2.5 KV and the impedance matched (50 $\Omega$ ) collector or anode of each MCP is at ground potential. The potential difference between the deflection grids is less than 1 kV.

The rectangular solid state detector is also used to measure the residual energy of the ions and is coupled through a network of high voltage capacitors and diodes to its charge sensitive amplifier. The fast analog electronics, described in more detail below, are housed in boxes surrounding the TOF vs E detector.

### Description of the Analog Electronics

The function of the analog electronics associated with the CHEM sensor is to measure the time-of-flight of the ions being analyzed (the time interval between signals of SEDA's A and C or between signals of SEDA's B and C), and to pulse-height analyze the output of the solid state detector D (see Fig. 12 for the physical locations of the SEDA's and the solid state detector in the CHEM sensor). In addition, a variety of coincidence conditions are established and a number of single, double, and triple coincidence rates ( a total of 6) are generated. The power requirement of the CHEM instruments is  $\sim 2500$  mW.

The block diagram of the analog electronics is shown in Fig. 13. The output of each of the three SEDA assemblies is fed directly into the respective constant fraction discriminator (CFD). The CFD output signals are used to trigger the appropriate one shots (as shown in the diagram), establish coincidences and increment the associated rate accumulators in the Data Processing Unit (DPU). A signal from either of the two CFD's connected to SEDA A and B respectively causes the time-to-amplitude converter (TAC) to start; a signal from the CFD of SEDA C stops the conversion. The TAC output pulse, whose amplitude is proportional to the time elapsed between the start and stop triggers, is pulse-height-analyzed by the analog-to-digital converter (ADC). The calibrate pulse generator (CPG) periodically triggers all three CFD's simultaneously, calibrating the TAC for zero time lapse.

The output of the solid state detector is coupled through a capacitor and diode network to a low noise charge sensitive preamplifier (CSA) followed by a pulse shaping amplifier (PSA) and threshold discriminator (DISCR). The signal from the amplifier is also fed into the second ADC for pulse-height analysis. Pulse trains from the two ADC's as well as the various counting rates are transferred to the data processing unit (DPU) for further analysis. It should be noted that pulse-height-analysis of the TAC output will occur in the absence of a signal from the solid state detector.

Two types of counting rates are generated. The three fast singles rates, (C1, C2 and C3) with a pulse-pair resolution of about 10 ns are multiplexed and prescaled prior to transfer to the DPU. The slower coincidence rates (C1·C3, C2·C3, C1·C3·D, C2·C3·D) and the solid state detector singles rate D ( $\sim 0.3$  to  $0.4$   $\mu$ s pulse-pair resolution) are fed directly into the DPU.

### Fast Electronics

As we have shown in Fig. 7, the output signal from the microchannel plates is fast ( $\sim 2$ ns) and its amplitude large ( $\sim 150$  mV). This simplifies considerably the design of the fast electronics and eliminates, for example, the requirements for fast preamplifiers. It also makes it possible to use emitter coupled fast linear IC's (ECL), thereby reducing weight and power requirements. The constant fraction discriminator poses the most difficult

**Block Diagram**  
**CHARGE-ENERGY-MASS (CHEM) SPECTROMETER**

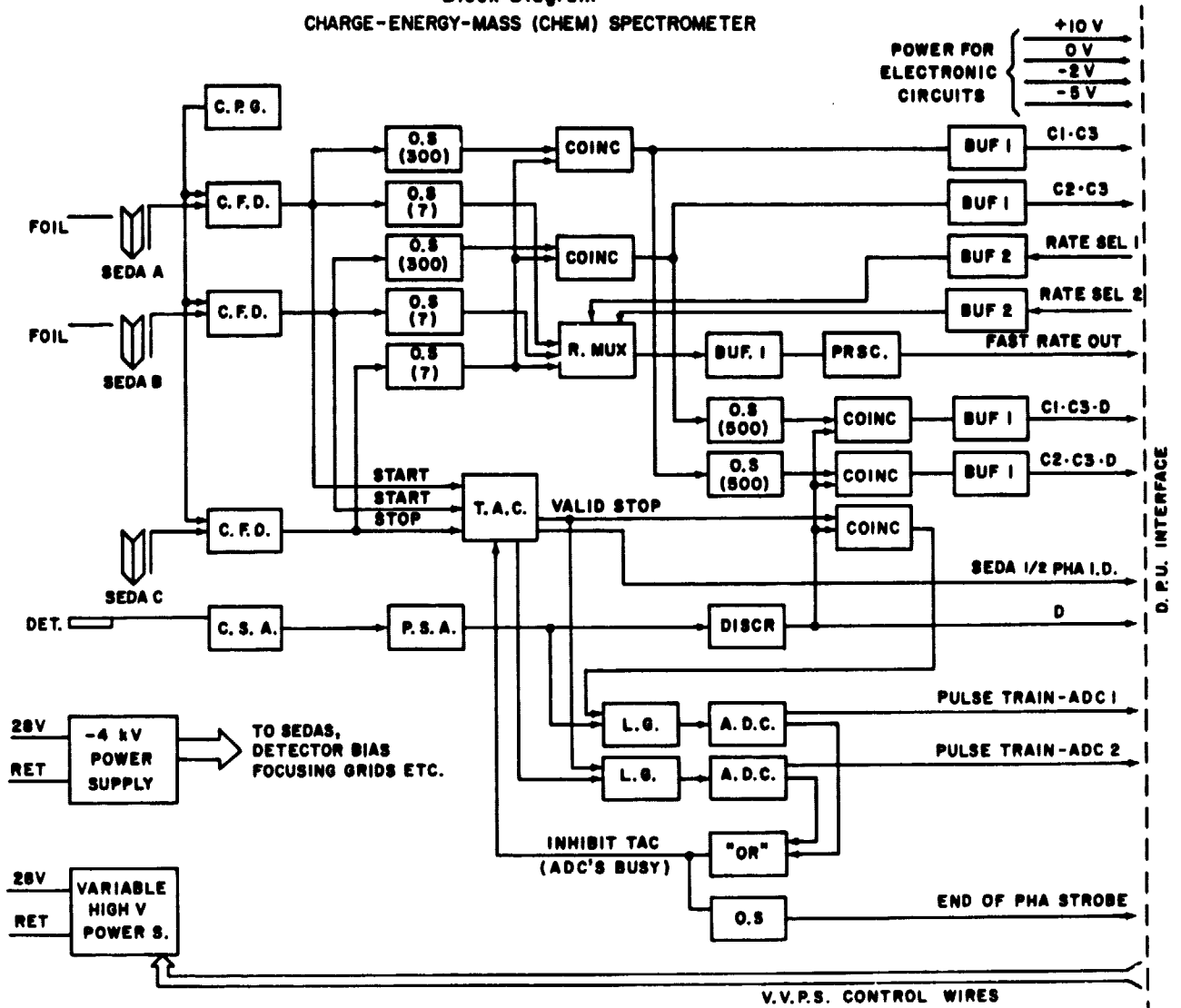


Fig. 13 Block diagram of the analog electronics associated with the CHEM spectrometer. The notation is: CPG - Calibrate Pulse Generator; CFD - Constant Fraction Discriminator; CSA - Charge Sensitive Amplifier; OS - One Shot (number in parenthesis is the pulse-width in nanoseconds); PSA - Pulse Shaping Amplifier; TAC - Time-To-Amplitude Converter; COINC - Coincidence Circuit; R.MUX - Rate Multiplexer; LG - Linear Gate; BUF. 1 - Type 1 Interface Buffer. Inputs from ECL circuits, outputs to TTL or PMOS circuits; DISCR - Amplitude Discriminator; ADC - Analog to Digital Converter; "OR" - "OR" - Gate; PRSC - Low power Schottky TTL prescaler; BUF. 2 - Type 2 Interface Buffer. Inputs from PMOS or TTL circuits, outputs to ECL circuits; SEDA - Secondary Electron Detector Assembly; DET - Solid State Au-Si Detector.

design and layout problem. This type of discriminator is widely used for fast timing applications (Gedcke and McDonald, 1968) and produces a time signal which accurately represents the onset time of the input pulse irrespective of its amplitude. The schematic diagram of a constant fraction discriminator breadboarded and tested in our laboratory is given in Fig. 14. The power consumption of this circuit is  $\sim 200$  mW and its only active component is a single MECL 10216 integrated circuit. The wave-forms shown on top are somewhat idealized; a careful layout is required to prevent "ringing". The voltage labeled "REF" is obtained directly from one of the pins of the IC.

### CONSTANT FRACTION DISCRIMINATOR

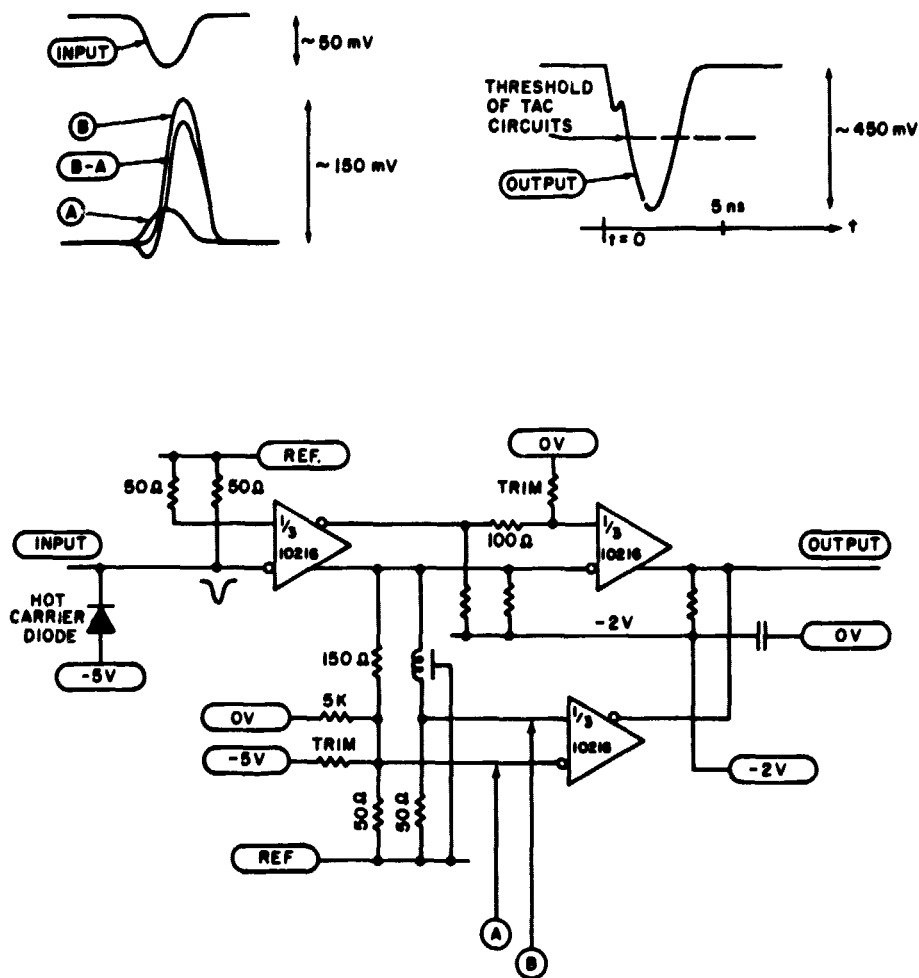


Fig. 14 Schematic diagram and sample pulse shapes for the Constant Fraction Discriminator using one MECL integrated circuit.

Using this circuit we have obtained an overall timing resolution of  $\approx 1$  ns FWHM for the time-of-flight measurement. Although this CFD will operate with an input signal whose amplitude is at least 50 mV, it is, of course, easy to increase this threshold an arbitrary amount by attenuating the input signal.

### High Voltage Supplies

The variable and 4 kV voltage supplies are existing designs used in the MPI/University of Maryland experiments on ISEE and similar to supplies we developed for the University of Maryland experiments on IMP's 7 and 8 (Tums, et al., 1974). In the variable deflection supply the output voltage is incremented at a rate selectable by ground command which may be as fast as one step/sec, between about 400 and 3000V. At each step the voltage is increased by a constant fraction, which is also adjustable. For example, the voltage range may be spanned by 32 or 64 logarithmically spaced steps.

The 4 kV supply is used to properly bias the foil (or solid state detector), the accelerating and deflection grids and the MCP's of the SEDA's. Taps on the intermediate stages of the adder chain provide all of the required voltages.

### Post-Acceleration

In order to extend downward the energy range of the CHEM Spectrometer (into region C of Fig. 11), the ions must be accelerated after they pass the deflection analyzer but before they enter the TOF vs E detector. A 30 kV post-acceleration is sufficient. In the configuration of the CHEM sensor which includes post-acceleration, shown in Fig. 15, the entire TOF vs E detector and analog electronics (except the variable power supply) are at the -30 kV potential. Physically, this high voltage "bubble" is isolated by a 1 cm gap from the grounded outer enclosure surrounding it. Three high-voltage stand-offs and two high-voltage feed-throughs (not shown) mechanically support the "bubble" so that the two entrance slits of the TOF vs E sensor line up opposite the two respective exit slits of the electrostatic analyzer.

A 30 kV high voltage supply of the same design as the University of Maryland 25 kV supply which has been fabricated and flight-qualified for the MPI/University of Maryland experiments on the ISEE A and C spacecraft, keeps the "bubble" at the high potential. This supply has field correction rings to prevent field emission discharge and is not potted or sealed in a dielectric gas. The power to the electronics in the "bubble" is supplied by means of an isolation transformer capable of withstanding 50 kV. Only digital logic signals will be transferred from the "bubble" to the DPU through the isolation transformer. The additional weight and power required to incorporate the post-acceleration in the CHEM spectrometer are  $\approx 1000$  gm and  $\approx 500$  mW respectively.

### On-Board Data Processing

In exploratory investigations it is highly desirable to have designed sufficient flexibility into the experiment to be able to change its mode of operation and match the observing program to the conditions which are encountered. The basic data provided by the CHEM spectrometer lend themselves to straight-

forward on-board processing which increases substantially the amount of information obtained on particle composition in a short time at limited telemetry rates. It is also easy to select different modes of operation and to implement a flexible observation program for CHEM which best fits the actual conditions encountered. It is easy to take advantage of these features of the CHEM by properly designing the Data Processing Unit.

### CHARGE-ENERGY-MASS (CHEM) SPECTROMETER

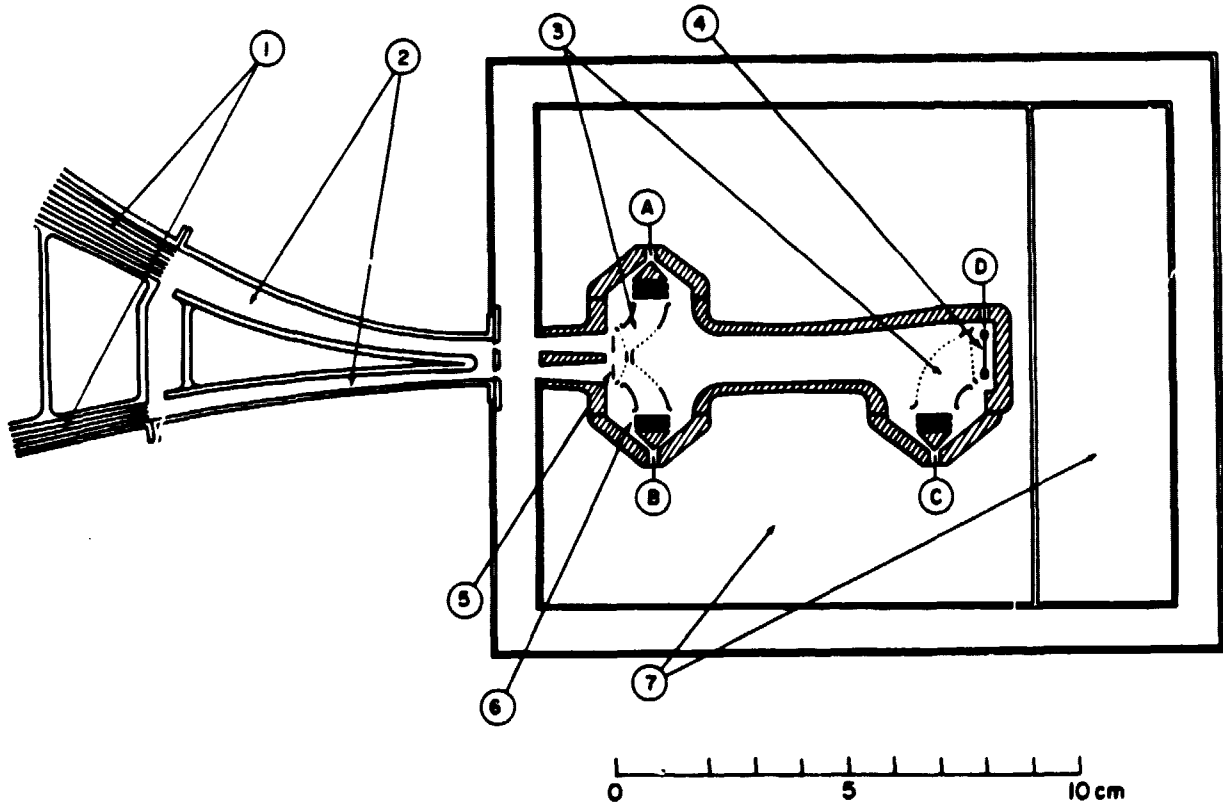


Fig. 15 Simplified cross-section of the CHEM sensor which includes post-acceleration. The high voltage "bubble" is separated from the grounded outer housing and the deflection analyzer by a 1 cm gap. The notation is identical to that of Fig. 12.

In Table 2 we list the data output of the CHEM spectrometer. The basic data, consisting of a 28 bit pulse-height word and counting rates, is telemetered at a nominal rate of about one "event" per second and provides the primary data base from which the absolute fluxes, energy spectra and the detailed charge state, chemical and isotopic composition of the thermal or suprathemal ions is determined.

TABLE 2  
Data Output of the CHEM Spectrometer

A. BASIC DATA

1. Pulse Height Analysis

	<u>No. of Bits</u>
Time-of-Flight	10
Energy	12
Angular Sector	4
Flags	2
High or Low Energy	
Double or Triple Coincidence	
	28 bits

2. Rates

	<u>No. of Accumulators</u>
Singles	
3 fast (10 ns, multiplexed and prescaled)	1
1 slow (1 $\mu$ s)	1
Double Coincidence	2
Triple Coincidence	$\frac{2}{6}$

B. ON-BOARD PROCESSED DATA

1. Particle Rates

	<u>No. of Accumulators</u>
4 non-sectored	4
1 sectored (16 sectors), or	16*
2 sectored (8 sectors)	$\frac{20}{20}$

2. Mass Spectra

	<u>No. of Accumulators</u>
16 Channels @ 24 bits	16*

\*Shared Accumulators

It is possible, however, to do in addition straight-forward on-board computation of the mass of the ions, information which may then be used instantly to make on-board selection of data to be transmitted to earth. For an idealized response of the TOF vs E detector, the mass  $m$  of the particle is related to the time-of-flight  $\Delta t$  and energy  $E$  by the expression

$m = a(\Delta\tau)^{\alpha}E^{\beta}$  where "a" is a constant determined by the geometry of the system  $\alpha = 2$  and  $\beta = 1$ . The actual measured response of the detector as shown in Fig. 10 does not change the form of the expression above but changes the values  $\alpha$  and  $\beta$ . A reasonable fit to the  $\Delta\tau$  vs  $E$  curves of Fig. 10 for elements above He is obtained with  $\alpha = 3$  and  $\beta = 1.3$ . Using table-look-up computational techniques, the mass of the particle may be computed on-board in  $\xi$  ms. This information can then be used to generate the "on-board processed data", listed in Table 2, which will enable one to

- (a) study simultaneously time variations (on a scale of 10's of sec) in the intensity of up to 4 elements or groups of elements (for example for H, He<sup>3</sup>, C to O and Na), and
- (b) examine angular distributions in 16 sectors for a given element or group of elements, or
- (c) accumulate a mass spectrum (on a time scale of 10's of sec) as a function of the particle energy or arrival direction.

The on-board computation of mass also makes it possible to select (by ground command) an ion species for high-priority analysis. Pulse-height information generated by this preferred ion species would be transmitted at the highest priority, making detailed composition studies of rare isotopes and elements feasible.

In addition to the priority selection based on the computed mass of the ion, a fast ( $\sim\mu$ s) decision on whether or not to analyze a given element can be made based on the value of the sum signal  $S = \Delta\tau + a \cdot E$  (see Fig. 9 and accompanying discussion) and on the state of the High/Low Energy Flag (SEDA 1/2 PHA ID signal of Fig. 13). In Table 3A we list the nominal priority selection for pulse-height analysis for both the fast ( $\sim\mu$ s) and slower ( $\sim$ ms) decisions based on energy and mass values of the incident ions.

The frequency and nature of data read out as well as a representative listing of ground commands are also given in Table 3B and 3C. The accumulation of counting rates is synchronized with the deflection voltage stepping and with the spin period of the spacecraft. The nominal readout frequency for the case of one voltage step on every spacecraft revolution is 12 pulse height events and 28 rate registers per revolution which is equivalent to about 75 bits/sec. In this mode the entire energy range of CHEM would be covered in about 6 to 7 min. It is of course, possible to change by ground command the voltage stepping rate and stepping sequence, as well as the priority for pulse-height analysis, select either angular sectoring or the accumulation of mass spectra, and select ion species for pitch angle distribution and rapid time variation analysis. This flexibility allows adjustment in near real-time of the mode of data collection to the varying condition and environments encountered.

#### Characteristics and Capabilities of the CHEM Spectrometer

The CHEM spectrometer described in the previous sections will measure at a bit rate of about 75 bits/sec the energy spectra of thermal or suprathemal ions on time scales ranging from minutes to days. Complete differential energy spectra for up to five different ion species may be obtained within  $\sim 5$  min., and the complete angular distribution of one ion species can be

recorded in less than a minute. It is important to note that at any given voltage step two-point differential energy spectra are measured for all ions which are within the energy range of CHEM and which satisfies the priority conditions. Availability of higher bit rates will result in obtaining complete measurements on shorter time scales.

TABLE 3  
Modes of Operation and Data Flow of the CHEM Spectrometer

---

A. PRIORITY SELECTION AND CYCLING FOR PULSE-HEIGHT ANALYSIS

Fast ( $\sim 1\mu s$ ) selection based on:

Mass of particle m: (5% for  $m \geq 1$ , 20% for  $m > 1$ , 75% for  $m > 4$ )

Energy of particle, E: (50% for  $E \lesssim 70$  keV/q, 50% for  $E \gtrsim 70$  keV/q)

Slow ( $\sim 1ms$ ) selection based on:

Mass of particle or group of particles (high priority for pulse-height analysis of elements in a mass range selected by ground command)

B. DATA READOUT FREQUENCY

- Data accumulation is synchronized with deflection voltage stepping.
- Voltage is stepped after an integral number of spacecraft spins.
- For voltage stepped once per spin, a representative data readout frequency would be

1 voltage and other ID	8
12 PHA events (28 bits each)	336
3 - 16 bit accumulators (fast rates)	48
9 - 12 bit accumulators (slower rates)	108
16 - 24 bit accumulators (sectored rate or mass spectrum)	<u>384</u>
	884 bit/revolutions

C. GROUND COMMANDS

On/Off SEDA A  
SEDA B  
Deflection Voltage

Mode Change

- Voltage stepping sequence and rate of stepping
  - Priority selection
  - Selection of mass spectra or angular sectoring
  - Selection of particle rates (sectored and non-sectored)
  - Selection of threshold levels on SEDA's and solid state detector
  - Change of SEDA bias level
-

## Charge and Mass Resolution

It is possible to calculate the charge and mass resolution of the CHEM Spectrometer using (a) the measurements of the energy loss and energy spread of ions in the carbon foils and solid state detectors (Figs. 5 and 6, in particular), (b) the characteristics of the MCP output and of the fast electronics, and (c) geometry of the CHEM sensor. The charge and mass resolution capabilities of the CHEM spectrometer can also be judged from Fig. 9 which shows that every charge state of every isotope of H and He is clearly resolved.

Since  $q = \alpha E'/\rho$  (see Fig. 1), the FWHM resolution of the charge state  $\Delta q$  will depend on the energy resolution of the analyzer  $\Delta\rho/\rho$  and the measured energy spread in the solid state detector  $\Delta E'$  as given in Fig. 5

$$(\Delta q/q)^2 = (\Delta E'/E)^2 + (\Delta\rho/\rho)^2.$$

The energy spread due to energy straggling of ions passing through the foil ( $\approx 3$  keV for He,  $\approx 10$  keV for Fe) is negligible compared to  $\Delta E'$  which ranges from 12 to  $\approx 300$  keV (see Fig. 5). For example, using the equation above and data from Figs. 5 and 6 we find that for 20 keV/q  $\text{He}^+$ ,  $\Delta q = 0.61$  while for 100 keV/q  $\text{O}^{+6}$  ( $\Delta\rho/\rho = 0.18$  above 70 keV/q)  $\Delta q/q = 0.20$  or  $\Delta q = 1.2$  charge units FWHM. At first glance it would seem that individual charge states would not be resolved in the latter case. One should remember, however, that in this case the energy is measured more accurately in the solid state detector (8%) than it is determined by the analyzer (18%) and that statistical analysis of the pulse-height data will improve the resolution of individual charge states in this region.

The mass resolution is more difficult to analyze since it depends also on the accuracy of the velocity measurements (the time-of-flight,  $\Delta\tau$ ). Contributing to the uncertainty in  $\Delta\tau$  are (a) flight-path uncertainties introduced by the finite area of the carbon foils and solid state detector ( $\approx 1.7\%$ ); (b) timing resolution of the electronics ( $\approx 1$  ns); and (c) time-of-flight dispersion of secondary electrons in the SEDAs ( $\approx 0.5$  ns). The largest contribution to the mass uncertainty comes from measurements of the ion energy.

In Fig. 16 we show sample calculations of the FWHM mass resolution capability of the CHEM spectrometer as a function of energy, taking into account all possible contributions to the mass uncertainty. The discontinuity in the curves for elements with  $m \lesssim 20$  is related to the considerable improvement obtained when the charge state of the ion has been determined. In such cases one can use the well defined values of  $\rho$  of the deflection analyzer instead of the more uncertain energy measured by the solid state detector to calculate the mass of the particle:  $m = 2q(\Delta\tau)^2/d^2$ .

The capability of the CHEM spectrometer to unambiguously resolve the charge states and isotopes of H and He is particularly noteworthy. For example,  $^2\text{H}/^1\text{H}$  ratio as low as  $10^{-5}$  are easily measured. We note from Figs. 16 and 9 that the mass resolution for H is about 0.1 amu so that a spillover of the more abundant  $^1\text{H}$  into  $^2\text{H}$  is for all practical purposes eliminated.

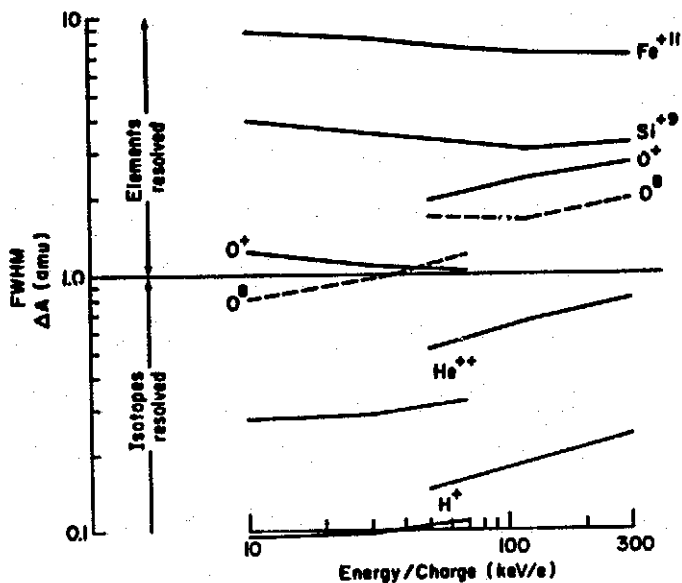


Fig. 16 Calculated mass resolution of the CHEM spectrometer as a function of energy. Isotopes of H and He are easily resolved. Individual elements up through oxygen are also separated as are the major elements beyond oxygen (Ne, Si, S, Fe).

#### Sensitivity, Geometrical Factors, and Detection Efficiency

The sensitivity (minimum fluxes measured) of the CHEM spectrometer depends on the value of the geometrical factor and the energy bandwidth of the analyzer, on the efficiency for detecting particles in the TOF vs E detector and on levels of accidental coincidence counting rates (background).

The multi-slit focusing collimators used in University of Maryland experiments (IMP 7 and 8, ISEE A and C) make it possible to obtain large geometrical factors without sacrifices in the energy resolution of the deflection analyzer. Although precise calculations of the geometrical factors of our deflection analyzers require Monte-Carlo computations, we can estimate the approximate magnitude of the geometrical factor  $G$  using the simple expression

$$G = n(s^2/\ell) (S_1 S_2/L),$$

where  $n$  is the number of slits in the collimator,  $s$  and  $S_1$  are the slit width and slit length respectively and  $\ell$  is the depth of the collimator,  $S_2$  is the width of the exit slit, and  $L$  the distance between the back side of the collimator and exit slit. Using representative values of  $N = 25$ ;  $s = 0.013$  cm;  $S_1 = 5$  cm;  $S_2 = 1$  cm;  $\ell = 3$  cm;  $L = 7$  cm, we find that  $G = 10^{-3}$  cm<sup>2</sup>sr for the high energy section, and (with  $n = 50$ )  $G = 2 \times 10^{-3}$  for the low energy deflection region. These estimates are valid to within a factor of 2.

In the TOF vs E detector the overall efficiency for detecting ions is the product of the efficiency of detecting an ion with the SEDAs (counting efficiency) and the fraction of ions which reach the stop SEDA after passing the carbon foils. We have measured the counting efficiency of heavy ions in our SEDAs to be  $\approx 95\%$  for He and heavier ions. (These values are consistent with the results shown in Fig. 8 on the pulse-height spectra of the SEDA.) Scattering of ions in the carbon foils prevents all ions which enter the TOF vs E detector from reaching the solid state detector. The scattering of ions is the result of multiple coulomb interactions of the ion with the carbon

nuclei in the foil, and the amount of scattering is inversely proportional to the energy per charge of the ion. From our measurements of the mean scattering angles for heavy ions in a  $5.5\mu\text{g}/\text{cm}^2$  carbon foil (Kirschner, 1975) we estimate that for the geometry of the TOF vs E system used in the CHEM spectrometer design (Fig. 12) between 10% and 50% of the ions going through the foil will reach the solid state detector.

The factor F (which, when multiplied by the number of ions of a given species detected by the CHEM spectrometer per unit time gives the absolute differential flux of these ions) is inversely proportional to the geometrical factor G, the counting efficiency  $\epsilon$  and fraction f of ions reaching the solid state detector, and the energy per charge bandwidth of the deflection analyzer,  $\Delta E/q$ . For the low energy deflection section, F values range between  $(2 \text{ and } 10) \cdot 10^4 \rho^{-1}$  and for the high energy section these values vary between  $(1.1 \text{ and } 5.6) \cdot 10^4 \rho^{-1}$ , where  $\rho$  is in units of keV/q. The variability in F is of course related to the amount of scattering of the ions and must be measured for each ion species using the actual geometrical configuration of the CHEM spectrometer.

The minimum ion intensities detected by the CHEM spectrometer are directly related to the background rate of the TOF vs E detector. Since in general the accidental double and triple coincidence rates of CHEM are extremely low, the minimum flux levels range from  $(0.1 \text{ to } 1) \rho^{-1} (\text{cm}^2 \text{ sec sr keV/q})^{-1}$ , where  $\rho$  is in units of keV/q. For example the minimum intensity of deuterium which can be measured with the CHEM spectrometer is  $\sim 10^{-2} (\text{cm}^2 \text{ sec sr keV})^{-1}$  at 20 keV and  $\sim 3 \cdot 10^{-4} (\text{cm}^2 \text{ sec sr keV})^{-1}$  at 300 keV. For elements heavier than Ne these values would be increased by about a factor of 5. We point out that priority selection will allow preferential analysis of rare isotopes and elements.

## V. OPERATION OF THE CHEM SPECTROMETER IN HIGH INTENSITY RADIATION ENVIRONMENTS

Intense fluxes of energetic charged particles (such as in the Jovian radiation belts) place severe requirements on electronic components and detector systems to simply survive effects of this radiation. To perform, in addition, meaningful measurements at these high intensity radiation levels a variety of techniques must be used to reduce the radiation background in the detector system to acceptable levels. The radiation induced background in the CHEM Spectrometer is reduced to negligible levels (even at Jupiter at  $6R_J$ ) by a combination of the following techniques.

- shielding of individual detectors in all directions against  $\leq 10$  MeV electrons and  $\leq 55$  MeV protons.
- electrostatic filtering which prevents electrons below 10 MeV and all ions, whose energies lie outside the narrow energy passband of the deflection analyzer, from reaching the TOF vs E detector.
- threshold discrimination on the output signals of the microchannel plates, which reduces substantially the detection efficiency for penetrating ( $>10$  MeV) electrons reaching the MCP.
- fast double and triple coincidence requirements which drastically reduce the accidental coincidence rate.
- two-dimensional pulse-height analysis which leads to further suppression of any residual background and makes it possible to correct for it.

## Background Levels Under Most Intense Radiation

We consider here the worst-case condition at Jupiter at 6  $R_J$  and will demonstrate that the CHEM spectrometer will operate properly in this environment and measure the energy spectra, and the charge states, isotopic and chemical composition of thermal or suprathreshold ions.

With a shielding of  $\sim 6$  gm/cm<sup>2</sup> surrounding the entire TOF vs E detector (see Figs. 12 or 15), the fluxes of penetrating electrons ( $>10$  MeV) and protons ( $>55$  MeV) are  $1.5 \cdot 10^7$  and  $<10^4$  (cm<sup>2</sup>sec)<sup>-1</sup> respectively (see "Jupiter Charged-Particle Environment for Jupiter Orbiter Probe 1981/1982 Mission, JPL publication 660-24, August 1976, hereafter referred to as Document 660-24). The counting rate in the MCP resulting from these penetrating particles is  $r_{MCP} = (1.5 \cdot 10^7 \epsilon_e + 10^4 \epsilon_p) A/2$  counts/sec, where A is the area of the MCP and  $\epsilon_e$  and  $\epsilon_p$  are the counting efficiencies for electrons and protons in the MCP above some threshold on the output signal. From Fig. 8 we may take as upper limits  $\epsilon_e = 3 \cdot 10^{-3}$  and  $\epsilon_p = 10^{-1}$ . Since the area of the MCP is 0.5 cm<sup>2</sup>,  $r_{MCP} \leq 10^4$  counts/sec. For the solid state detector (area 0.85 cm<sup>2</sup>) the efficiency for counting electrons and protons is close to 1 and the maximum counting rate  $r_D$  at 6  $R_J$  is  $r_D \leq 6.5 \cdot 10^6$  counts/sec.

We now estimate the accidental double ( $r_d$ ) and triple ( $r_t$ ) coincidence rates for the TOF vs E detectors.  $r_d = (r_{MCP})^2 \tau_{TAC}$ , where  $\tau_{TAC} = 3 \cdot 10^{-7}$  sec is the maximum on-time for the time-to-amplitude converter (TAC). Since  $r_{MCP} \leq 10^4$ ,  $r_d \sim 30$  counts/sec. Similarly,  $r_t = r_d r_D (\tau_D + \tau_{TAC}) \sim 2 r_d r_D \tau_{TAC} \sim 120$  counts/sec.

Pulse-height analysis allows further suppression of background. The  $\sim 1000$  channel time-of-flight pulse-height spectrum of the background produced by accidental coincidences would be flat (due to their random nature) with the number of background counts/channel/sec,  $R_d = r_d/10^3$ . The background contribution in the region of the TOF pulse-height spectrum corresponding to the actual time-of-flight of ions traversing the TOF system (typically 3 to 30 channels, or 1 to 10 ns) will therefore be  $(r_d/10^3) \cdot 10$  or  $\sim 0.3$  counts/sec. For the two-parameter pulse-height analysis of TOF vs E signals, the corresponding number is 0.1 counts/sec. From this we conclude that the minimum intensity for a given ion species (such as Na<sup>+</sup>) which can be measured reliably at 6  $R_J$  using the CHEM spectrometer varies between  $\sim 10^2$  (cm<sup>2</sup>sec sr keV/q)<sup>-1</sup> at 300 keV/charge and  $6 \cdot 10^4$  (cm<sup>2</sup>sec sr keV/q)<sup>-1</sup> at 1 keV/charge.

## Background Levels Due to Spacecraft RTG's and RHU

Spacecraft used for Outer Planets Missions rely for their power and heat sources on Radioisotope Thermoelectric Generators (RTG's) and Radioisotope Heater Units (RHU's). Contributions from the RTG and RHU generated neutron and gamma flux must be considered. Using flux values of 80 and  $3.2 \times 10^3$  (cm<sup>2</sup>sec)<sup>-1</sup> for neutron and gamma radiation from the RTG and RHU (see "Orbiter Description Document for Jupiter Orbiter Probe 1981/1982 Mission, JPL publication 660-22, August 1976, p. D-16) we estimate the counting rates in the MCP and the solid state detector to be  $r_{MCP} \leq 50$  counts/sec and  $r_D \ll 100$  counts/sec. Here we assumed that the efficiency of the MCP for detecting gammas is about the same as the counting efficiency for 400 keV electrons ( $\sim 3 \cdot 10^{-3}$ ). The background rates are estimated to be  $r_d \leq 8 \times 10^{-4}$  and  $r_t \leq 5 \times 10^{-8}$  counts/sec, and are entirely negligible.

## Consideration of Effects Due to Spacecraft Charging

At Jupiter spacecraft charging up  $\sim 10$  to  $-20$  kV will accelerate the Jovian thermal plasma (ions) to  $>10$  keV/charge. This pre-acceleration will of course destroy any spectral features of the initially thermal plasma (it would only be seen at one value of the deflection voltage of the CHEM spectrometer), but should not affect the charge state, isotopic and chemical composition of these ions. It is estimated that the maximum expected intensity of accelerated thermal Jovian ions (at  $\sim 6R_J$ ) is  $\leq 2 \cdot 10^9 / (\text{cm}^2 \text{sec sr})$  using information provided in Table 6-1 of Document 660-24. The expected maximum counting rate in the start SEDAs of the TOF vs  $\frac{1}{2}$  detector will be  $\leq 2 \cdot 10^6$  counts/sec, well within the capabilities of the CHEM fast ( $\sim$ ns) electronics which can handle rates of  $\geq 2 \cdot 10^7$  counts/sec. More typical counting rates produced by the pre-accelerated ions are in the range of  $\sim 2 \cdot 10^5$  to  $\leq 2 \cdot 10^4$  counts/sec. Even if a Jupiter Orbiter spacecraft remained charged at  $-10$  kV or more for a whole year (a most unlikely situation) the expected fluence at the solid state detector would be  $\leq 3 \cdot 10^{12}$ , a level which is considerably lower than the  $10^{13}$ - $10^{18}$  value at which degradation in solid state detector noise characteristics begins to take place.

## VI. EFFECTS OF RADIATION ON THE LONG-TERM PERFORMANCE OF THE CHEM SPECTROMETER

The individual detector elements in the CHEM Spectrometer which may be affected by exposure to the high intensity radiation are (a) the carbon foils, (b) solid state detector, and (c) microchannel plates. We will consider each in more detail below using the Jovian radiation environment as a model for the high intensity radiation. The fast-time electronics (primarily ECL IC's are known to be radiation resistant.

### Carbon Foils

Thin carbon foils are commonly used as targets in low energy nuclear experiments where they are routinely exposed to intense beams of energetic ions. It is typically observed (Stoner, 1976) that  $5 \mu\text{g}/\text{cm}^2$ , 5 mm diameter unsupported carbon foils will survive a 3 MeV,  $\mu\text{A}$   $\text{N}^+$  beam from a Van de Graaff for more than 30 min. From this information we can estimate the foil lifetime in a high intensity radiation environment (such as at Jupiter). It is reasonable to assume that the lifetime will depend on the total amount of energy ( $E_T$ ) deposited in the foil, where  $E_T = N_T(dE/dx) \Delta x_{\text{foil}}$  and  $N_T$  is the total number of  $\text{N}^+$  ions hitting the foil in  $\sim 2000$  sec at 1  $\mu\text{A}$  beam current. For 3 MeV  $\text{N}^+$ ,  $dE/dx = 9 \text{ keV}/\mu\text{g}/\text{cm}^2$  (see Fig. 6),  $N_T = 6.4 \cdot 10^{16}$  and  $E_T = 2.9 \cdot 10^{18} \text{ keV}/\text{cm}^2$ . At Jupiter at  $6R_J$  the shielded carbon foils will see penetrating electrons ( $\geq 10 \text{ MeV}$ ) and protons ( $\geq 55 \text{ MeV}$ ) at intensities of  $1.5 \cdot 10^7$  and  $< 10^4 \text{ cm}^{-2} \text{sec}^{-1}$  respectively. Since the average energy losses for electrons and protons at these energies are  $2 \cdot 10^{-3}$  and  $2 \cdot 10^{-2} \text{ keV}/\mu\text{g}/\text{cm}^2$  respectively (Barkas and Berger, 1964; Berger and Seltzer, 1964), the energy deposited in the foil by these penetrating particles is  $1.6 \cdot 10^5 \text{ keV}/\text{cm}^2 \text{sec}$ . Even in this extremely high intensity radiation the foils would survive  $2 \cdot 10^{13}$  sec or  $6 \cdot 10^5$  years.

The maximum foreground rate is expected for a Jupiter orbiter spacecraft when it is charged to  $-10\text{kV}$  or more. It has already been shown that the maximum rate in the carbon foils is, under these conditions,  $2 \cdot 10^6$  counts/sec. Since the energy loss of 10 to 20 keV protons is  $\sim 1 \text{ keV}/\mu\text{g}/\text{cm}^2$  in carbon (see Fig. 6) and the foil area is  $0.2 \text{ cm}^2$ , the energy deposited in the carbon foil is  $5 \cdot 10^7 \text{ keV}/\text{cm}^2\text{sec}$ . Even at this maximum proton intensity the foil lifetime would exceed  $5 \cdot 10^{10} \text{ sec}$  or  $1.5 \cdot 10^3 \text{ years}$ .

### Solid State Detectors

Surface barrier solid state detectors exposed at their front surface (Au) to  $\sim 200 \text{ keV}$  protons will not change their noise characteristics below fluence levels of  $10^{13}/\text{cm}^2$  (Coleman et al., 1968). The onset of degradation is expected to occur even at higher fluence levels when these detectors are exposed to penetrating protons and electrons. Solid state detectors have of course been flown on the Pioneer 10, 11 missions, where they have survived large radiation doses, and are used extensively in MJS77 experiments.

The solid state detector in the TOF vs E detector of the CHEM Spectrometer may see a foreground proton intensity of  $\sim 10^6/\text{cm}^2\text{sec}$  (when the spacecraft is charged to  $-20\text{kV}$ ). Since these particles will enter the system only at one value of  $\rho = E/q$  of the analyzer, (about 3% of the time), the total fluence in one year would be  $\lesssim 10^{12}/\text{cm}^2$  under these most extreme conditions. This fluence level is below the  $10^{13}/\text{cm}^2$  at which degradation begins to set-in. We may therefore safely conclude that the solid state detector in the CHEM Spectrometer will easily survive the Jovian radiation environment.

### Microchannel Plates

There are two published reports on the lifetime of microchannel plates under high intensity irradiation (Ruggieri, 1972; Sandel et al., 1976). Ruggieri (1972) finds that, similar to channeltrons, microchannel plates exposed to irradiation have long periods of stable gain operation after an initial reduction in gain (to  $\sim 0.8$  to  $0.4$  of initial gain, depending on the microchannel plate used). Sandel et al. (1976), on the other hand, see a continuing drop in gain as the duration of exposure is increased. The relevant number to calculate is the accumulated charge density at the chevron microchannel plate assembly output due to its exposure to the Jovian radiation. In Table 4 are listed representative fluences of electrons ( $\gtrsim 10 \text{ MeV}$ ) as a function of radial distance from Jupiter for a Jupiter orbiter spacecraft. The total fluence  $F$  below  $16 \text{ R}_J$  is  $\lesssim 8 \cdot 10^{11}/\text{cm}^2$ . Relating this to the accumulated charge density  $Q$  at the output of the MCP assembly we find  $Q = F \epsilon g e = 6.4 \cdot 10^{-3} \text{ coul}/\text{cm}^2$ .  $\epsilon$  is the efficiency of detecting penetrating electrons and was taken to be  $0.1$  (Ruggieri, 1972),  $g$  is the gain of the chevron microchannel plate assembly (taken to be  $10^6$ ) and  $e$  is the electron charge in coulombs. Exposures of channel plates to radiation which produce  $Q$  levels of  $\sim 6 \cdot 10^{-3} \text{ coul}/\text{cm}^2$  reduces their gain to values between  $0.6$  and  $0.98$  of their original gain (Ruggieri, 1972; Sandel et al., 1976). The observed variability in the gain change is apparently related to the fabrication history of a particular channel plate. Even though changes in gain by a factor of 2 can be tolerated in the present application of the MCP's, screening and selection of MCP's should yield devices which have long term gain stability.

TABLE 4

Fluence of Electron  $\lesssim 10$  MeV Between 6 and 16 R<sub>J</sub>\*

R <sub>J</sub>	Intensity (cm <sup>2</sup> sec) <sup>-1</sup>	Time (Hours)	Fluence (cm <sup>2</sup> )
6-7	1.5·10 <sup>7</sup>	9	4.9·10 <sup>11</sup>
7-8	1.1·10 <sup>7</sup>	4	1.5·10 <sup>11</sup>
8-9	7·10 <sup>6</sup>	3.7	9.3·10 <sup>10</sup>
9-10	3·10 <sup>6</sup>	3.4	3.7·10 <sup>10</sup>
10-11	8·10 <sup>5</sup>	3.3	9.5·10 <sup>9</sup>
11-12	2·10 <sup>5</sup>	3.3	2.4·10 <sup>9</sup>
12-13	1.1·10 <sup>5</sup>	3.3	1.3·10 <sup>9</sup>
13-14	1·10 <sup>5</sup>	3.3	1.2·10 <sup>9</sup>
14-15	7·10 <sup>4</sup>	3.3	8.3·10 <sup>8</sup>
15-16	5·10 <sup>4</sup>	3.3	5.9·10 <sup>8</sup>
Total Fluence	7.83·10 <sup>11</sup> /cm <sup>2</sup>		

\* Date derived from Documents 660-21 and 660-24

To compensate further for any gain changes in the MCP's it is possible to incorporate in the design provisions for changing the MCP bias levels by ground command. For example, with the ability to increase the bias voltage on the rear MCP of the chevron assembly by 50% (from 650 to 1000V) constant gain can be maintained in the MCP even at fluence levels of  $\sim 5 \cdot 10^{13}$ /cm<sup>2</sup>.

Additional shielding will also significantly reduce the fluence levels seen by the TOF SEDA's. For example, increasing the thickness of the shield to  $\sim 13$  gm/cm<sup>2</sup> would exclude  $\lesssim 40$  MeV electrons from reaching the MCP and thus reduce the fluence by a factor of  $\sim 80$ . The weight penalty for the extra shielding is about 600-700 gm.

## VII. OPERATION OF THE CHEM SPECTROMETER IN THE SOLAR WIND

The intensity of solar wind protons is typically  $\lesssim 10^8 \text{ cm}^{-2} \text{ sec}^{-1}$  although values as high as  $\sim 10^9 \text{ cm}^{-2} \text{ sec}^{-1}$  have been observed during disturbed periods. In this section we will demonstrate that the CHEM spectrometer is capable of measuring the charge states, isotopic and chemical composition and energy spectra of heavy ions in the presence of large solar wind proton fluxes. We note at this time that these peak intensities are observed by the CHEM spectrometer only at a few of the voltage steps of the deflection analyzer and only when the instrument points along the solar wind flow direction. The fraction of time when both conditions occur is typically less than 1%.

### Background Caused by Solar Wind Protons

Since the  $m/q$  ratio of protons is smaller than that of all other ions, it follows that for a given value  $\rho = E/q$  of the deflection analyzer (same energy per charge) (a) protons are deflected more than all other ions, and (b) they travel faster than all other ions. A straight-forward way to eliminate protons from analysis would be to electronically by-pass the few voltage steps ( $\rho$  values) at which solar wind protons would enter the TOF detector. It should be recognized that this would not eliminate analysis of other solar wind ions which enter the TOF system at different deflection voltages. However, as we show below, the CHEM Spectrometer will operate properly even when solar wind protons enter the TOF detector.

The counting rate,  $r_p$ , produced by solar wind protons in the start SEDA is  $r_p = A_s T \epsilon_p f_p = 5 \cdot 10^6 \text{ cts/sec}$ , where  $A_s$  is the area of the exit slit ( $0.1 \text{ cm}^2$ ),  $T$  is the parallel transmission of the focusing collimator (0.5),  $\epsilon_p$  is the efficiency for detecting protons in the start SEDA ( $\epsilon_p = 0.1$ , see Fig. 8), and  $f_p$  is the peak proton flux ( $f_p \lesssim 10^9 \text{ cm}^{-2} \text{ sec}^{-1}$ ). Because protons which enter the TOF detector (even after they are post-accelerated) travel faster than all other ions [ $v_p/v_i = (m_i/q_i)^{1/2}$ ], all time-of-flight measurements triggering by protons will always be stopped by protons. These time-of-flight intervals will be  $\lesssim 40 \mu\text{s}$ , which is the time-of-flight of a solar wind proton post-accelerated by 30 kV. At a rate of  $5 \cdot 10^6 \text{ cts/sec}$  these protons will cause at most a 20% dead time in the electronics. The high priority selection based on the amplitude of the time-of-flight signal,  $\Delta\tau$ , can be used to effectively exclude pulse-height analysis of solar wind protons, without affecting measurements of their intensity, velocity, density and temperature.

Even while solar wind protons are analyzed in the TOF detector, the CHEM Spectrometer is sensitive to all other ions over 80% of the time. The background rate caused by solar wind protons stopping the time-of-flight analysis started by other ions is given by  $r_B = r_i r'_p (\Delta\tau_i - \Delta\tau_p) < r_i$ .  $\Delta\tau_i$  is the time-of-flight of these ions ( $< 200\text{ns}$ )  $r_i$  is the rate at which they trigger the start SEDA,  $\Delta\tau_p$  is the time-of-flight of protons (10 to 40ns) and  $r'_p (< r_p)$  is the rate in the stop SEDA due to solar wind protons. Pulse-height analysis of the time-of-flight and energy signals further suppress the background by at least a factor of 100, resulting in a "signal-to-noise" ratio of over 100 in the region of the  $\Delta\tau$  vs  $E$  matrix corresponding to the location of the "real ion events".

## Effects of Solar Wind Protons on the Long-term Performance of the CHEM Spectrometer.

We have shown in the previous section that solid state detectors and microchannel plates will operate without degradation at fluence levels below  $\sim 10^{13}/\text{cm}^2$  and  $8 \cdot 10^{11}/\text{cm}^2$  respectively. By incorporating provisions to increase the bias voltage on the rear MCP of the SEDAs it is possible to maintain constant gain operation even to fluence levels of  $5 \cdot 10^{13}/\text{cm}^2$ . The yearly fluence level,  $F_S$ , at the solid state detector of the CHEM spectrometer due to solar wind protons is  $F_S = n r_p f_t = 3 \cdot 10^{11}$  where  $n = 3 \cdot 10^7$  sec/yr,  $r_p \sim 5 \cdot 10^6$  protons/sec (assuming an average intensity of  $10^8 \text{ cm}^{-2} \text{ sec}^{-1}$ ) and  $f_t = 2 \cdot 10^{-3}$  is the fraction of time solar wind protons enter the TOF system. The corresponding yearly fluence level,  $F_{MCP}$ , at the microchannel plates is  $F_{MCP} = 3 \cdot 10^{10}$  where  $r_p$  was taken to be  $5 \cdot 10^5$  cts/sec. Since these fluences are 20 to 30 times below the levels at which degradation begins it can be concluded that solar wind protons will not affect the long-term performance of the CHEM Spectrometer even on  $\sim 10$  year missions.

## VIII. PRESENT STATUS OF DEVELOPMENT OF THE CHEM SPECTROMETER

The CHEM Spectrometer is designed using detectors and components each of which has flown on previous space missions as will be demonstrated below.

### Deflection Analyzer

The electrostatic deflection analysis of energetic particles using large-area multi-slit focusing collimators and high voltage (up to  $\sim 15$  kV) deflection supplies has been used by the University of Maryland group in their IMP 7 and 8 experiments (Tums *et al.*, 1974) which are still operating and returning data of excellent quality. The deflection analyzer and stepped deflection supply of CHEM are direct adaptations of the existing and flight-qualified deflection system of the MPI/University of Maryland ISEE A and C experiments.

### Rectangular Solid State Detector

Rectangular solid state detectors have been fabricated at the University of Maryland since 1968. None of the 25 solid state detectors in the Maryland IMP experiments has failed. For the ISEE experiments we have fabricated and flight qualified low noise (5 keV FWHM), thin window ( $19 \mu\text{g}/\text{cm}^2$  Au) rectangular ( $0.3 \times 2$ )  $\text{cm}^2$  solid state detectors. The requirements for the solid state detector used in CHEM are similar to these ISEE detectors.

### Secondary Electron Detector Assembly (SEDA)

The essential components of the SEDA are the 5 (and 10)  $\mu\text{g}/\text{cm}^2$  grid supported carbon foils, the chevron microchannel plate assembly and the high voltage ( $\sim 4$  kV) bias supply. The University of Maryland group has flown 5, 10 and 15 kV supplies in their IMP 7 and 8 experiments. All these supplies are still functioning properly.

Thin carbon foils are surprisingly strong and extremely durable. This accounts for the fact that they are commonly used in low energy nuclear physics experiments. 2  $\mu\text{g}/\text{cm}^2$  carbon foils have been flown successfully on rocket experiments (Bernstein *et al.*, 1969a, b), and grid supported, 5 and 10  $\mu\text{g}/\text{cm}^2$  carbon foils have passed MJS level vibration tests (Hsieh, 1976). We have shown in section VI that carbon foils, as configured in CHEM will easily survive the most intense radiation environment.

Microchannel plates are mostly used as image intensifying devices, and are commercially available in the standard circular as well as rectangular configurations of most any reasonable size. Chevron microchannel plate assemblies have flown on rockets (Kellogg, *et al.*, 1976; Lampton, 1976) and are an integral component of the Ultraviolet Spectrometer experiment on the Mariner Jupiter/Saturn (MJS77) Mission (Sandel *et al.*, 1976). In Sections VI and VII, it was demonstrated that features incorporated in the CHEM Spectrometer design (shielding, bias adjustment) will assure the stable operation of the chevron MCP assemblies in the most intense radiation environment (at 6R<sub>J</sub> at Jupiter) and in the solar wind.

#### Time-of-Flight vs Energy Detector

Time-of-flight is a powerful technique of mass identification of low energy particles which has been used in a variety of nuclear physics experiments (Goulding and Harvey, 1975; Viola 1976). In Section III we summarized our own work during the past two years using this technique, and presented results of calibrations of a prototype TOF vs E detector using ion beams.

#### Electronics

The constant fraction discriminator which uses one MECL IC (see Section IV) has been breadboarded and tested. Because of the very modest requirements for the fast electronics ( $\sim 1$  ns FWHM timing resolution using  $\sim 2$  ns,  $>150$  mV input pulses) this CFD circuit only requires  $\lesssim 200$  mW power. The other fast electronics circuits (time-to-amplitude converter, coincidence, calibrate pulse generator) are currently being designed.

#### 30 kV Supply

The University of Maryland group has had extensive experience in designing and fabricating low-power, ultra high voltage supplies and associated high voltage components for the MPI/University of Maryland experiment on the ISEE A and C spacecraft. A20 to 25 kV (adjustable) deflection supply has been built and flight-qualified. The -30 kV supply to be used in the thermal plasma version of the CHEM Spectrometer will be similar to the ISEE 25 kV supply except for field correction rings to prevent any field emission discharge. The -30 kV supply and the power and signal isolation transformer are currently being designed.

**Acknowledgements**

The development of the CHEM Spectrometer as well as its testing is supported by the National Aeronautics and Space Administration under grants NGR-21-002-224 and NGR 21-002-316. The development for flight of focusing multi-slit collimators, stepped deflection analyzers and high voltage ( $\sim 25$  kV) supplies has been funded by NASA under contract NAS5-11063 and NAS5-20062. We are particularly grateful to E. Tums, who is developing the fast-time electrons, and to J. Cain, who is responsible for the mechanical design. R. Lundgren, M. McMillan, P. Kirschner and R. Lambird contributed effectively in developing and calibrating the time-of-flight detector during the past two years. Special thanks go to Steve Brown who not only provided us with excellent beams of heavy ions but also made numerous helpful suggestions during calibration runs.

## REFERENCES

- Barkas, W.M., and M.J. Berger, Tables of Energy Losses and Ranges of Heavy Charged Particles, NASA Publication, NAS SP-3013, 1964.
- Berger, M.J., and S.M. Seltzer, Tables of Energy Losses and Ranges of Electrons and Positrons, NASA Publication, NAS SP-3012, 1964.
- Bernstein, W., A.J. Cole, R.L. Wax, Penetration of 1-20 keV Ions Through Thin Carbon Foils. Nuc. Inst. and Meth., 90, p. 325, 1970.
- Bernstein, W., G.T. Inouye, N.L. Sanders, and R.L. Wax, "Measurements of Precipitated 1-20 keV Protons and Electrons During a Breakup Aurora", JGR, 74, p. 3601 (1969a).
- Bernstein, W., R.L. Wax, N.L. Sanders, and G.T. Inouye, An Energy Spectrometer for Energetic (1-25 keV) Neutral Hydrogen Atoms, Small Rocket Instrumentation Techniques, (North-Holland Publ., Comp. Amsterdam, 1969b).
- Chu, W.K., P.D. Bourland, D.H. Wang, and D. Powers, Range and  $dE/dx$  of C, N, O, F and Ne in Be and C from 500 keV to 2 MeV, Phys. Rev., 175, 2, p. 342, 1969.
- Clerc, H.G., H.J. Gehrhardt, L. Richter, and K.H. Schmidt, Heavy-Ion Induced Secondary Electron Emission - A Possible Method for Z-Identification, Nuc. Instr. and Meth., 113, p. 325, 1973.
- Eberhardt, P., The Solar Wind as Deduced from Lunar Samples, Solar Wind Three, C.T. Russell, ed., p. 58, 1974.
- Fritz, T.A., Ion Composition, International Symposium on Solar Terrestrial Physics (ISSTP), Boulder, Colorado, June 7-18, 1976.
- Gedcke, D.A. and W.J. McDonald, Design of the Constant Fraction of Pulse Height Trigger for Optimum Time Resolution, Nuc. Inst. and Meth., 58, p. 253, 1968.
- Gloeckler, G., Low Energy Particle Composition, Proc. 14th International Cosmic Ray Conference, Munich, W. Germany, August 15-29, Vol. II, p. 3784, 1975.
- Goulding, F.S. and B.G. Harvey, Identification of Nuclear Particles. Ann. Rev. of Nuc. Sci., 25, p. 201, 1975.
- Green, M.I., P.F. Kenealy, and B.G. Beard, Fast-Timing Measurements Using a Chevron Microchannel Plate Electron Multiplier. Nuc. Inst. and Meth., 126, p. 175, 1975.
- Hirschberg, J., Coronal and Solar Wind Abundances, Solar Wind Three, C.T. Russell, ed., p. 26, 1974.

Hogberg, G., Electronic and Nuclear Stopping Cross Sections in Carbon for Light Mass Ions of 4.5 to 4.6 keV Energy. *Phys. Stat. Sol. (b)*, 48, p. 329, 1971.

Hsieh, K.C., (private communication), 1976.

Ipavich, F.M., R.L. Lundgren, B.A. Lambird, G. Gloeckler, Measurements of Pulse Height Defect in Silicon for Ions with  $Z \lesssim 36$  from  $\sim 2$  to  $\sim 400$  keV/nuc. (to be published), 1977.

Kellogg, E., P. Henry, S. Murray, L. Van Speyberok, and P. Bjorkholm, *Rev. Sci. Instr.*, 47, p. 282, 1976.

Kirschner, P.E., A Time of Flight Detector, M.S. Thesis, University of Maryland (unpublished) 1975.

Lampton, M., Microchannel Plates and Their Applications to Photon Counting Image Systems, IAU Colloquium No. 40, (Paris), 1976.

Lindhard, J., M. Scharff, and H.E. Schiott, Range Concepts and Heavy Ion Ranges, *Mat. Fys. Medd. Dan. Vid. Selsk.*, 33, No. 14, p. 1, 1963.

Meyer, J.P., Isotopic Composition of Cosmic Rays. 14th International Cosmic Ray Conference, Munich, W. Germany, August 15-29, Vol. II, p. 3698, 1975.

Northcliffe, L.C. and R.F. Schilling, *Nuclear Data Tables, A*, 7, p. 233, 1970.

Ormrod, J.H. and H.E. Duckworth, Stopping Cross Sections in Carbon for Low-Energy Atoms with  $Z = 12$ . *Can. J. Phys.*, 41, p. 1424, 1963.

Powers, D. and W. Whaling, Range of Heavy Ions in Solids. *Phys. Rev.*, 126, 1, p. 61, 1962.

Ruggieri, D.J., Microchannel Plate Imaging Detectors. *ISEE Trans. on Nuc. Sci.* NS-19, No. 3, p. 74, 1972.

Sandel, B.R., A.L. Broadfoot, and D.E. Schemansky, Microchannel Plate Lifetests, submitted to *Applied Optics*, 1976 (preprint).

Schneider, W.F.W., B. Kihlmeyer, and R. Bock, Mass-Identification of Alpha-Particles and Heavy Ions by Time-of-Flight Methods, *Nuc. Instr. and Meth.*, 87, p. 253, 1970.

Soul, P.B., Operational Properties of Channel-Plate Electron Multipliers. *Nuc. Instr. and Methods*, 97, p. 555, 1971.

Stoner, (private communication), 1976.

Tums, E., G. Gloeckler, C.Y. Fan, J. Cain, and R. Sciambi, Instrument to Measure Energy and Charge of Low Energy Interplanetary Particles, ISEE Trans. Nucl. Sci., NS-21, No. 1, 210, 1974.

Viola, V., (private communication), 1975.

Washington, D., Improving the Resolution of High Gain Channel Plate Arrays for Particle and Photon Counting. Nuc. Inst. and Meth., 111, p. 573, 1973.

Wijngaarden, A.V. and H.E. Duckworth, Energy Loss in Condensed Matter of  $H^1$  and  $He^4$  in the Energy Range  $4 < E < 30$  keV. Can. J. Phys., 40, p. 1749, 1962.